Title

Prefrontal-insular gamma synchrony promotes modality-specific cognitive flexibility

ISBN

9798247949688

Author

Hagopian, Lara Louise

Publication Date

2026-06-03

Peer reviewed|Thesis/dissertation

Prefrontal-insular gamma synchrony promotes modality-specific cognitive flexibility

by

Lara Louise Hagopian

THESIS

Submitted in partial satisfaction of the requirements for degree of

DOCTOR OF PHILOSOPHY

in

Neuroscience

in the

GRADUATE DIVISION

of the

UNIVERSITY OF CALIFORNIA, SAN FRANCISCO

Approved:

DocuSigned by: Kevin Yackle
863799D3911346A...

Kevin Yackle
Chair

DocuSigned by:
D52E8F0D49433...

Mazen Kheirbek

DocuSigned by:
0AE4A64E0BF472...

Massimo Scanziani

DocuSigned by:
70A483C8DEB04E6...

Vikaas S. Sohal

Committee Members

Dedication

To my mother, father, and sister for all their endless love and support.

Acknowledgements

It is because of my surrounding scientific community that made this project possible.

I would like to thank my former mentors and lab mates that encouraged me to pursue my PhD and my friends within the community for going through this journey together.

Thank you to my thesis committee members for all their helpful advice.

A special thank you to the Sohal lab and especially Dr. Vikaas Sohal for being invaluable in helping, mentoring, and molding the scientist I am today.

Prefrontal-insular gamma synchrony promotes modality-specific cognitive flexibility

by

Lara Louise Hagopian

Abstract

The ability to alter our behavior based on sensory inputs, such as odors or textures, is a necessity for adaptation. The medial prefrontal cortex (mPFC), important for cognitive function,[1] produces gamma synchrony that is necessary for this behavioral flexibility in a Rule-Shifting task tested in mice.[7-9] It is unclear what other regions contribute to the cognitive flexibility needed for this task. The insula is known to be necessary for proper cognitive function[20, 33,41] and also has bidirectional connectivity with the mPFC.[20] Here we apply optogenetic inhibition on the medial insular cortex (mIC) to mPFC projecting (mIC-mPFC) cell bodies and terminals during a Rule-Shifting task in mice to show that this projection is necessary for texture to odor cue rule shifts. We further determine the existence of gamma synchrony between mIC and mPFC parvalbumin interneurons (PVIs) during this task and find a difference in synchrony based on the cue type using a novel recording technique called transmembrane electrical measurements performed optically (TEMPO).[31] This gamma synchrony was shown to be necessary for rule shifts to odor due to a deficit from out-of-phase optogenetic gamma stimulation. Overall, the results show the mIC is necessary for optimal rule shifting to an odor cue.

Table of Contents

List of Figures

Chapter 2

Chapter 3

Chapter 4

Chapter 5

List of Abbreviations

Claustrum (**CLA**)

Electroencephalography (**EEG**)

Fluorescence Mini-Cubes (**FMC**)

Genetically Encoded Voltage Indicators (**GEVIs**)

Initial Association (**IA)**

Insular Cortex (**IC**)

Local Field Potential (**LFP**)

Medial Insular Cortex (**mIC**)

Medial Prefrontal Cortex (**mPFC**)

mIC to mPFC projections (**mIC-mPFC**)

Odor to Texture (**O→T**)

Parvalbumin (**PV**)

Parvalbumin Interneuron (**PVI**)

Prefrontal Cortex (**PFC**)

Rule Shift (**RS**)

Texture to Odor (**T→O**)

Transmembrane Electrical Measurements Performed Optically (**TEMPO**)

Vesicular Glutamate Transporter (**VGLUT2**)

Wisconsin Card Sort Task (**WCST**)

Chapter 1

Introduction

Utilizing five senses, humans observe the continuously changing environment to build a model for the external world. We use sight, sound, taste, odor and tactile cues to detect changes in the environment, and adapt accordingly via cognitive flexibility. Whether it is experimenting with flower oils to create an irresistible perfume or letting the desire for a softer sweater lead to the creation of cashmere, we are constantly relying on these five modalities to note when the environment calls for a shift in behavior. Cognitive flexibility allows us to unlearn and relearn in new ways, or adapt, to continually evolve on a daily basis.

Understanding the process of adaptation, through cues, raises several questions. 1) What brain area(s) are responsible for cognitive flexibility? 2) How can we use behaviors to measure cognitive flexibility? 3) What are physiological correlates of cognitive flexibility? 4) Can we parse cognitive flexibility via different types of cues? 5) Do the brain regions necessary for the cognitive flexibility depend on the type of cue? Answering these questions to completion will take many years to come, however, later chapters will show a start in understanding cue modality-dependent cognitive flexibility.

One brain region frequently implicated in cognitive flexibility is the medial prefrontal cortex (mPFC).[1-8] The mPFC is involved in many forms of executive and cognitive functions such as working memory, memory recognition, emotional regulation, spatial cognition, planning, problem solving, along with cognitive flexibility.[1-13] It is thought to be the integrator of information for optimal decision making.[1,14-16] While it does not receive sensory input directly, it does receive information from regions, like the insular cortex that collect sensory information,[10,12,17-20] allowing the mPFC to respond to environmental cues.

Understanding how the mPFC incorporates cues of different modalities may give insight

on circuit mechanisms for cognitive flexibility. Studying this requires a behavioral test for cognitive flexibility that can separate the roles of different cue modalities.

In humans, cognitive flexibility can be studied using the Wisconsin Card Sort Task (WCST).[3,21-24] In this task, a subject is presented with three cards; each card displays symbols which vary in number, shape and color. A person must determine through trial and error of card selection if the number of symbols, their shape, or their color should be used for sorting; once this initial rule is learned, the rule changes, requiring the subject to shift attention to a different modality.

Individuals suffering from brain lesions in the PFC, Alzheimer's disease, schizophrenia, depression, anxiety, and bipolar disorder all exhibit impairments in cognitive flexibility reflected by deficits in WCST performance compared to healthy controls.[3,21-24] In addition, in some cases these deficits are associated with an impairment in a certain pattern of brain activity known as *gamma oscillations.* [25-28]

Gamma oscillations have been observed during various cognitive tasks including tasks which measure cognitive flexibility.[7-9,25-29] Gamma oscillations reflect rhythmic (30-100Hz) activity of neurons in a specific brain areas that produce a signal which can be measured through electroencephalography (EEG) or local field potential (LFP) recordings.[29] Gamma oscillations are known to be mainly generated by rhythmic firing of inhibitory interneurons, specifically parvalbumin interneurons (PVIs).[29,30] When two brain areas are producing gamma oscillations synchronously, it suggests that they may be potentially communicating or otherwise interacting.[29]

Previous work from our laboratory has observed disruptions in cognitive flexibility by disrupting gamma oscillations in the mPFC by targeting prefrontal PVIs in mice.[7-9] Studying the role of gamma oscillations and PVIs in cognitive flexibility, requires a task similar to the WCST, but suitable for mice, along with a recording technique that can measure rhythmic activity in specific cell types, like PVIs.

Our laboratory uses a mouse Rule-Shifting task that shares certain features with the WCST. This task uses odor and texture cues. On each trial, mice are presented with two bowls and must learn to dig in the bowl containing a specific cue (odor or texture) to obtain a hidden food reward. Once that initial association (IA) has been learned, the rule will change without warning to the other modality, and the mice must learn this rule shift (RS) (see figure 2.1 and methods for details).

To record from PVIs directly, we used Transmembrane Electrical Measurements Performed Optically (TEMPO).[31] TEMPO uses genetically encoded voltage indicators to measure voltage membrane dynamics at fast time scales comparable to LFP recordings, for specific cell types.[31] Previous work from our laboratory has used TEMPO to show that PVIs exhibit a significant increase in gamma synchrony between the mPFC hemispheres, specifically following error vs. correct trials during the Rule-Shifting task.[8,9] To determine the necessity of cross hemispheric gamma synchrony during a rule shift, PVIs in the mPFC received in-phase and out-of-phase 40Hz optogenetic excitation during the RS period; RS impairment was only observed during out-of-phase stimulation.[8] Out-of-phase stimulation during the IA period showed no impairment, implying cross hemispheric PVI gamma synchrony in the mPFC is specifically necessary during a rule shift, but not for learning a rule.[8] Disrupting gamma synchrony in the mPFC by unilaterally optogenetically inhibiting the long range projections of PVIs between mPFC hemispheres during a rule shift, also lead to behavioral impairment, emphasizing the necessity of these PVI callosal projections for optimal rule shifting.[9]

These results show that normal gamma oscillations are necessary for proper cognitive flexibility. It is possible other areas contribute to gamma synchrony in the mPFC, or synchronize with the mPFC via gamma oscillations to promote cognitive flexibility in the Rule-Shifting task. Therefore, to better understand how cognitive flexibility occurs, we have investigated the synchrony of gamma oscillations between the mPFC and other cortical regions during rule shifts based on specific cue modalities.

The ideal brain region to examine would be necessary for cognitive tasks, involved in processing odor or texture cues, and have connectivity with the mPFC. The insula (insular cortex, IC) is a region that encompasses all of these qualities and more.

The IC is known to be involved in functions such as somatosensation, interoception, salience processing, emotional processing, anxiety, social cognition, learning, memorizing valence, and decision making.[32-45] It has bidirectional connections throughout the cortex along with some subcortical, midbrain and hindbrain structures,[20] which supports the idea that it is involved in integrating information.[46] Understanding examples of the IC's circuit and involvement in learning, suggest it may be particularly critical for cognitive flexibility in the Rule-Shifting task.

First, stroke patients with a damaged IC have been shown to struggle with cognitive tasks, such as set-shifting.[47,48] Select human stoke patients with a lesion in the IC participated in a set-shifting task that was a shape-based Trail Making Test from the Oxford Cognitive Screen.[47] It involved participants to be presented with different sizes of squares and circles together; participants switch between matching large squares to small squares and large circles to small circles in descending order until all shapes have been matched.[47] Those with lesions in the left IC showed a deficit in this task.[47] The mPFC is also a region needed for optimal set-shifting[68].

Second, the IC is involved in cue learning. In a previous study using the classic Pavlovian paradigm, mice are presented with visual and auditory cues simultaneously to learn when to anticipate a reward by poking their head into a reward port; mice were thought to learn the cue when the number of head entries in the reward port would increase with the onset of the cues.[34] When the IC was pharmacologically or optogenetically inhibited, the mice struggled to learn the association and were less likely to anticipate the reward, showing the IC's importance in cue learning.[34]

Third, the insula is involved in taste and olfaction,[36,39] implying it may be involved in learning associations between odor cues and food rewards. Gustatory information is processed in the gustatory cortex that integrates taste and olfactory cues and even sends information to

the mPFC[67]; the gustatory cortex resides within the IC.[36,67] The IC has been shown to be involved in learning novel tastes; when mice are presented with novel tastes, the anterior IC to mPFC projection is necessary for a neophobic response and remembering of the novel taste.[41] The IC also has bidirectional communication with the olfactory cortex in mice.[20]

Fourth, the IC has extensive bidirectional connectivity with motor and somatosensory cortices,[20] raising the possibility that it may be involved in detecting specific textures in the Rule-Shifting task. Specifically, when comparing seventeen major regions' inputs and outputs of the IC, the somatosensory cortex sends the greatest amount of excitatory and inhibitory input to the IC while also receiving a large amount of the IC's output.[20]

Lastly, beyond its potential involvement with learning odors and textures, the IC also has a large amount of bidirectional connectivity with the mPFC[20]. Note, for all the regions the IC communicates with, the amount of this connectivity differs between the anterior, medial, and posterior IC.[20]

Therefore, given the IC involvement in learning, decision making, olfaction, tactile processing, and connection with mPFC, it is a promising candidate to manipulate and monitor during odor and texture shifts of the Rule-Shifting task.

In the following chapters, we will explore the contribution of medial insular cortex (mIC) projections to mPFC during the Rule-Shifting task. We found optogenetic inhibition of these cell bodies or terminals leads to performance deficits specifically during shifts to odor cues in this task. Gamma synchrony occurs between mIC and mPFC, specifically between PVIs in both regions, with different patterns of synchrony occurring when learning rule shifts to odor vs texture cues, emphasizing a difference in processing between these modalities. When gamma synchrony between the mIC and mPFC is disrupted, we see a deficit in rule shifts. We conclude, the mIC is necessary for learning shifts to odor based rules in the Rule-Shift task.

Chapter 2

mIC to mPFC projections

The following experiments attempt to reveal how the mIC interacts with the mPFC during the Rule Shifting task to determine its involvement in cue-dependent cognitive flexibility.

*mIC to mPFC projecting cell bodies are necessary for **ODOR** shifts*

We sought to determine the behavioral effects of inhibiting mIC to mPFC communication. We used optogenetic inhibition of mIC-to-mPFC-projecting (mIC-mPFC) cell bodies when mice were shifting to an odor cue during the Rule-Shift task.

Wild-type (WT) mice were injected with AAVrg-EF1a-Cre (AAVrg-cre; 'retro-cre') in mPFC and AAV5-Ef1a-DIO-eNpHR-eYFP (experimental group, 'eNpHR+') or AAV5-Ef1a-DIO-eYFP (control group, 'eYFP+') in mIC; optical fibers were implanted bilaterally in mIC (Fig. 2.1a-b). One concern may be that we are also targeting the claustrum (CLA); however, we see there is very little viral spread to the CLA; the fiber implant is also directly above the mIC, given the size/shape of the fiber and strength of the laser, light emitted from the fiber will mainly target the mIC; we will revisit the concern for the CLA in chapter 3.

Eight to nine weeks later, mice were run on the Rule-Shifting task for three days. Here, mice were presented with two bowls of textures and odors (sand, litter, garlic, coriander; Fig. 2.1c). Mice had to first learn a rule based on one modality (e.g., 'dig in garlic-containing bowl'), then shift to a rule of the other modality (e.g., 'dig in the sand-containing bowl'). These two rules represent the initial association (IA) and rule shift (RS) phases of the task, respectively (Fig. 2.1c, see methods for details). Mice were run for three days on this Rule-Shift task comprising both IA and RS phases (Day 1: texture to odor shift; Day 2: odor to texture shift; Day 3: texture to odor shift), receiving optogenetic inhibition on Day 3 specifically during the RS trials of the Rule-Shift task (Fig. 2.1c-d); optogenetic inhibition was turned off once mice were placed back

into the holding cage during intertrial intervals (including extended timeouts after error trials). We found there is a significant deficit in RS performance, as measured by the number of trials needed to reach the learning criterion (8/10 consecutive trials correct), during Day 3 for experimental (eNpHR+) mice compared to Day 1 ($p<0.0001$) and Day 2 ($p<0.0001$); there is also a significant difference between experimental (eNpHR+) and control (eYFP+) mice on that Day 3 ($p=0.0001$; Fig. 2.1d). Control (eYFP+) mice showed no significant difference in RS performance between Day 1 and Day 3 ($p=0.11$; Fig. 1d). Control (eYFP+) mice did show a slight, but significant, deficit in performance on Day 3 compared to Day 2 ($p=0.03$), but the experimental (eNpHR+) mice still perform markedly worse than controls (eYFP+) on Day 3 (Fig. 2.1d).

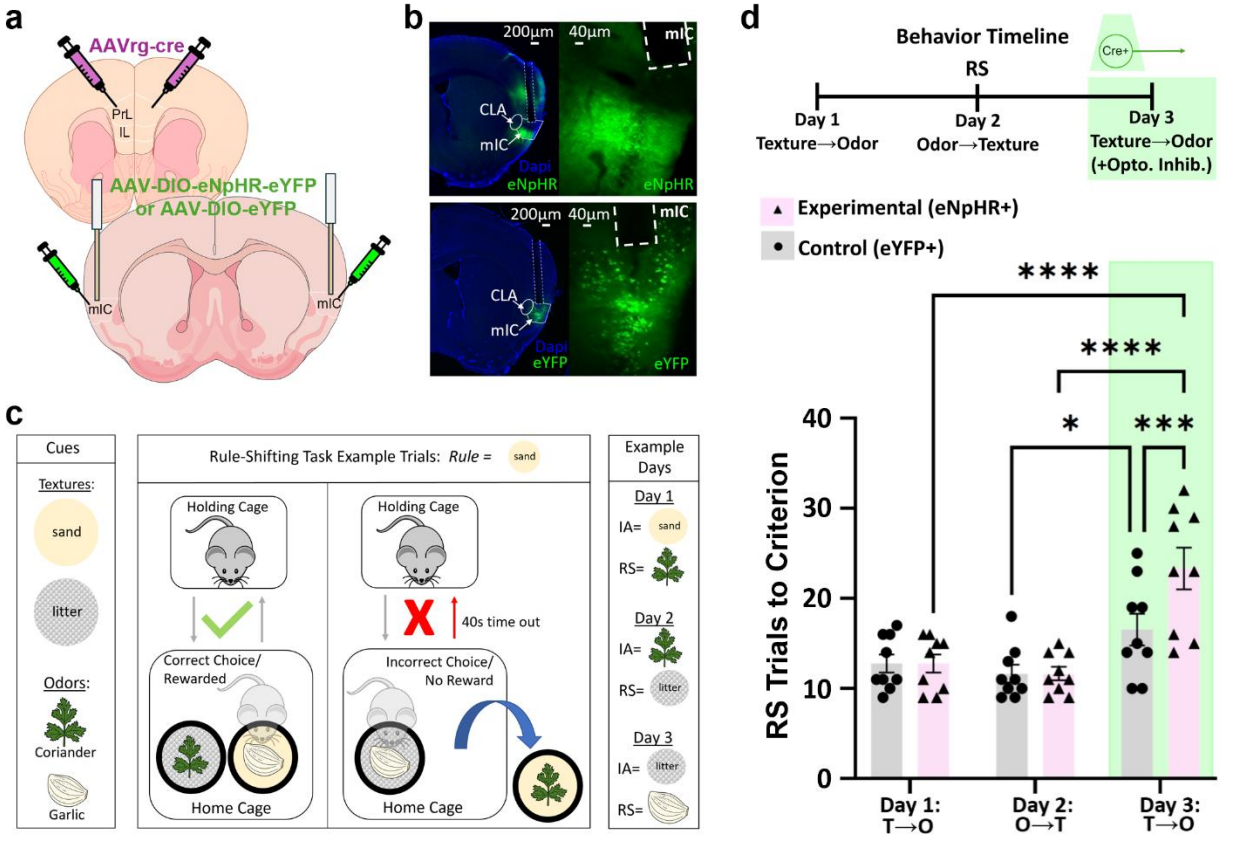

Figure 2.1*: Optogenetic inhibition of the mIC to mPFC projecting cell bodies leads to RS deficit during rule shifts to* ***ODOR****:* a)Surgery schematic of injection of AAVrg-cre was bilaterally injected into mPFC and AAV-DIO-eNpHR-eYFP or AAV-DIO-eYFP was injected with fiber implants bilaterally into mIC. b) Example of visualizing surgeries (eNpHR-eYFP top, -YFP bottom). c) Rule shifting schematic example: left is all possible cues; middle is an example of correct and incorrect trial if the rule is sand; the right is an example of what the rules could be across three day's, with the previous days RS as the following day's IA. *(Figure caption continued on next page.)*

(Figure caption continued from previous page) d) Top: the behavioral timeline where mIC to mPFC cell bodies are inhibited during each trial on day 3; bottom: there is significant deficit of during inhibition where mice struggle to learn the texture to odor shift compared to control days (Texture to Odor shift: T→O; Odor to Texture shift: O→T; Day 1: p=<0.0001, Day 2: p=<0.0001) and controls (p=0.0001).

This difference may be related to the fact that mice perform a shift to texture on Day 2 vs. to odor on Day 3. Another possibility is that light delivery in control (eYFP+) mice mildly impairs performance due to heating effects. Of note, implants in the mIC are very close to the striatum where light delivery has been shown to produce heat-related behavioral deficits[49]. We do not consistently observe this difference between Day 2 vs. Day 3 performance in control mice in later experiments.

Overall, these findings suggest that the mIC-mPFC neurons are necessary for rule shifts to odor. However, it begs the question, could inhibition of mIC to mPFC projecting cell bodies also lead to deficits when shifting to texture-based rules, and/or might we be impairing the ability of mice to detect or process odor cues more generally?

mIC-mPFC projection neurons are NOT necessary for texture shifts or initial learning of odor

We delivered optogenetic inhibition to mIC-mPFC projecting neurons when mice were shifting to a texture cue during the Rule-Shift task or when learning an initial odor cue.

Wild-type mice were injected and implanted the same as above (Fig. 2.1a-b). To determine if there would be a performance deficit during odor to texture shifts, mice were run for three days on the rule shift task(Day 1: odor to texture shift; Day 2: texture to odor shift; Day 3: odor to texture shift), receiving optogenetic inhibition on Day 3 during the RS trials of the Rule-Shift task (Fig. 2.2a); as before, optogenetic inhibition was turned off when mice were in the holding cage during intertrial intervals. There is no significant difference in learning (RS trials needed to reach learning criterion) on Day 3 (+ optogenetic inhibition) for experimental (eNpHR+) or control (eYFP+) mice compared to the other days. This suggests that, in contrast to shifts to odor-based rules, mIC-mPFC projection neurons are not necessary for shifts to texture-based rules.

To determine if inhibiting mIC-mPFC neurons more generally disrupts the ability of mice to detect, learn from, or make decisions based on odor cues, mice were run for two days on a version of the task where both Day 1 and Day 2 had a randomly assigned IA based on odor (Day 1: IA based on one odor cue; Day 2: IA based on the other odor cue). On Day 2, mice received optogenetic inhibition during IA trials (Fig. 2.2b); again optogenetic inhibition was turned off when mice were in the holding cage during intertrial intervals. While there was a main effect between Day 1 and Day 2 ($p=0.01$), we found no significant difference between Day 1 and Day 2 for experimental (eNpHR+) mice ($p=0.052$) or control (eYFP+) mice ($p=0.09$), nor a significant difference between experimental (eNpHR+) and control (eYFP+) mice when we delivered light for optogenetic inhibition on Day 2 ($p=0.42$).

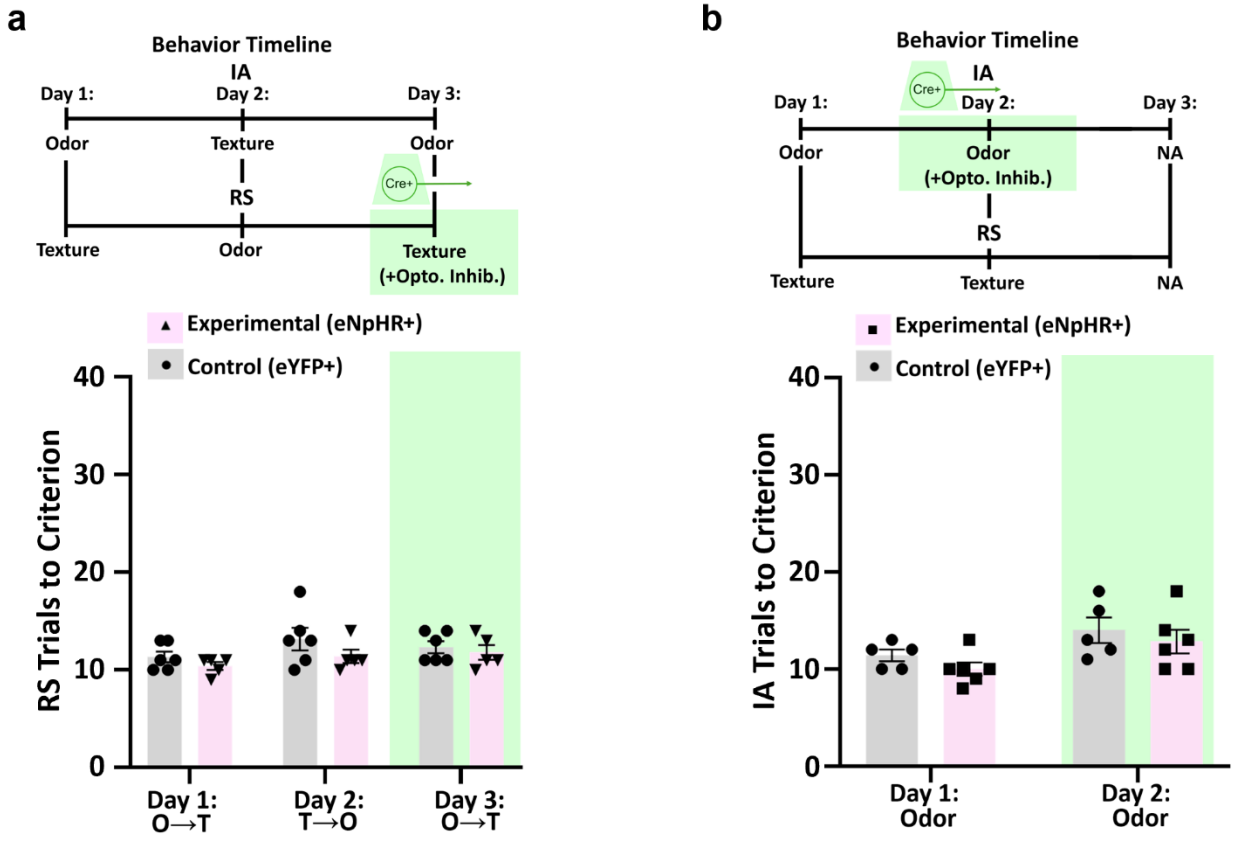

Figure 2.2: *Optogenetic inhibition of mIC to mPFC projecting cell bodies during RS does NOT affect texture shifts or the ability to learn an odor rule*: a) Top: the behavioral timeline for IA and RS where mIC to mPFC cell bodies are inhibited during each trial on day 3 during RS; bottom: there is no significant behavioral deficit during optogenetic inhibition for eNpHR+ vs eYFP+ compared to control days. b) Top: the behavioral timeline where mIC to mPFC cell bodies are inhibited during each trial on day 3 during IA; bottom: there is no significant behavioral deficit during optogenetic inhibition for eNpHR vs eYFP compared to control days.

*Optogenetic Inhibition of the mIC-mPFC **terminals** leads to RS Deficits during **ODOR** shifts*

While it is clear that mIC-mPFC neurons are necessary for texture to odor rule shifts, given the excessive output from the IC to the rest of the brain,[20] it is possible that these neurons mediate these effects through projections to other regions, besides mPFC. To confirm that the direct projection of mIC-mPFC neurons to mPFC is necessary, we delivered optogenetic inhibition to mIC-mPFC terminals within the mPFC when mice were shifting from texture to odor.

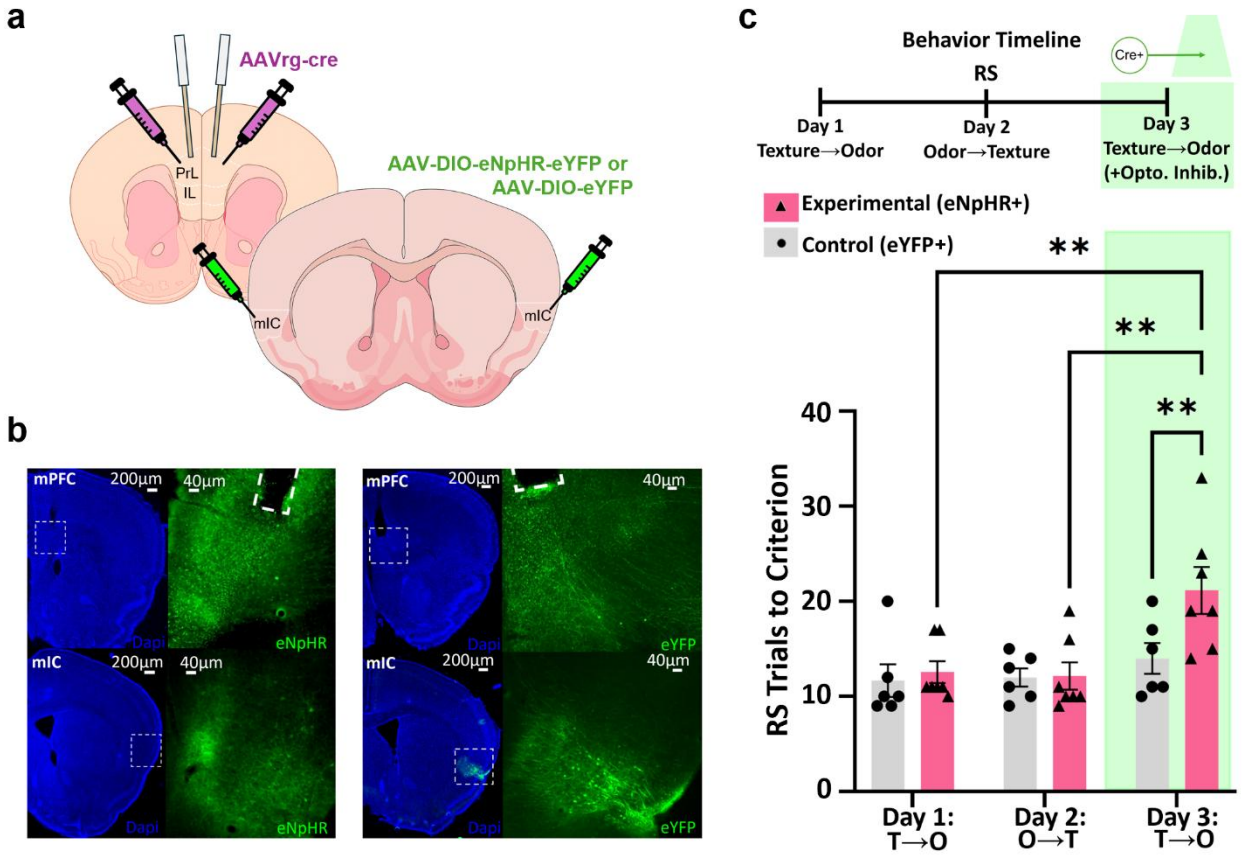

Figure 2.3: *Optogenetic inhibition of the mIC to mPFC projecting **terminals** leads to RS deficit during **ODOR** shifts*: a)Surgery schematic of injection of AAVrg-cre and fiber implants were bilaterally injected into mPFC and AAV-DIO-eNpHR-eYFP or AAV-DIO-eYFP was injected bilaterally into insula. b) Example of viral injection and implants (eNpHR+ on the left, eYFP+ right) from surgeries in (a). c) Top: the behavioral timeline where mIC to mPFC terminals are inhibited during each trial on day 3 during odor RS; bottom: there is significant deficit of during inhibition where mice struggle to learn the odor shift compared to control days (Day 1 vs 3: p=0.0019, Day 2 vs 3: p=0.0012) and compared to controls (p=0.0086) during odor RS.

Wild-type (WT) mice were again injected with AAVrg-EF1a-Cre (retro-cre) in mPFC and either AAV5-Ef1a-DIO-eNPHR-eYFP (experimental group, ‘eNpHR+’) or AAV5-Ef1a-DIO-eYFP (control group, ‘eYFP+’) in mIC; optical fibers were implanted bilaterally in mPFC (Fig. 2.3a-b).

Mice were run for three days on the Rule-Shift task (Day 1: texture to odor shift; Day 2: odor to texture shift; Day 3: texture to odor shift), and received optogenetic inhibition on Day 3 during RS trials (Fig. 2.3c); again optogenetic inhibition was turned off when mice were in the holding cage during intertrial intervals.

There was a deficit in learning, as evidenced by a significant increase in the number of RS trials needed to reach the learning criterion on Day 3 (+optogenetic inhibition) for experimental (eNpHR+) mice compared to Day 1 ($p=0.0019$) and Day 2 ($p=0.0012$); there is also a significant difference between experimental (eNpHR+) and control (eYFP+) mice on Day 3 ($p=0.0086$) (Fig. 2.3c). There is no significant difference for control (eYFP+) mice on Day 1 vs Day 3 ($p=0.58$) or Day 2 vs Day 3 ($p=0.67$) (Fig. 2.3c).

Chapter 3

Concern for the CLA?

The CLA is believed to act as a relay center between cortical regions[50,51] due to its extensive bidirectional connectivity with numerous regions, including the mPFC.[51-57] The CLA's strongest connections are with areas involved in higher order brain functions, like the mPFC.[8] In the mPFC specifically, the CLA is connected mostly to neurons in deeper layers, where the bulk of mPFC PV interneurons reside.[58,59] The CLA is also believed to be involved in attention[65] and possibly the transmission of neural synchrony.[60-62] Thus, the CLA is well-positioned to integrate diverse information from all other cortical regions, in order to dynamically filter salient information. One way the CLA may do this is by transmitting this filtered information to the mPFC in order to facilitate executive functions, potentially by modulating synchrony.

While synchronization between the CLA and other brain areas has not been demonstrated, the monosynaptic glutamatergic projections from CLA to mPFC PVIs[63,68] raise the possibility that it could entrain rhythmic activity in the mPFC or promote synchronization within the mPFC. In particular, the CLA excites mPFC PVI, which elicits feedforward inhibition within mPFC pyramidal neurons[58]; this is a potential mechanism through which CLA input could impact mPFC synchronization. Furthermore, there is a similar pattern of mPFC input eliciting feedforward inhibition in the CLA. Therefore, it is possible that by targeting PVI, the CLA may regulate gamma synchrony in the mPFC, with potential for a recurrent loop of circuitry between them.

The CLA has also been shown to be an important component in cue mediated behavior, like the mPFC. A study posted on bioRxiv examined the CLA and mPFC circuit. CLA neurons were targeted by using the vesicular glutamate transporter, (VGLUT2), encoded by the Slc17a6 gene,[63] which is thought to be expressed specifically in the CLA and not its surrounding regions.[64] It found that designer receptors exclusively activated by designer drugs (DREADDs)

mediated inhibition or continuous optogenetic excitation of the CLA can disrupt learning during a rule shift of a similar task to Rule-Shifting.[63] Note, all mice in this study switched from a texture to an odor on the day of inhibition or excitation.

Here we attempted to obtain similar results using our Rule-Shift task and optogenetics instead of DREADDs to inhibit CLA neurons.

CLA is not individually necessary for rule shifting

While our viral injections and light delivery should mainly target the mIC (Fig. 2.1a-b), it is still possible that the CLA contributes to the behavioral impairments we observed. Examining whether directly targeting the CLA elicits similar effects may help to resolve this issue.

We used Vglut2-ires-cre (Vglut2-Cre) mice, along with viral transfections, to target CLA neurons for optogenetic inhibition during our Rule-Shift task. Mice were bilaterally injected with AAV5-Ef1a-DIO-eNpHR-eYFP (experimental group, 'eNpHR+') or AAV5-Ef1a-DIO-eYFP (control group, 'eYFP+'), with bilateral implants above the CLA (Fig. 3.1a-b).

Just like the study above, mice were run on our Rule-Shift task for two days (Day 1: Odor to texture; Day 2: Texture to odor). Mice received continuous optogenetic inhibition on Day 2 during the RS period.

While there was a main effect between Day 1 and Day 2 ($p=0.02$), we found no significant difference between Day 1 and Day 2 for experimental (eNpHR+) mice ($p=0.09$), nor a significant difference between experimental (eNpHR+) and control (eYFP+) mice when we delivered light for optogenetic inhibition on Day 2 ($p=0.13$) (Fig. 3.1c). A significant difference in performance between Day 1 and Day 2 for control mice was found ($p=0.01$), likely driving the overall difference between Day 1 and Day 2.

As described previously, light delivery to the striatum has been shown to produce heat-related behavioral deficits[49]. For targeting the CLA, the fiber optic implant is near the striatum. Thus, it is possible that changes in performance from Day 1 to Day 2 reflect non-specific heating

effects caused by light delivery.

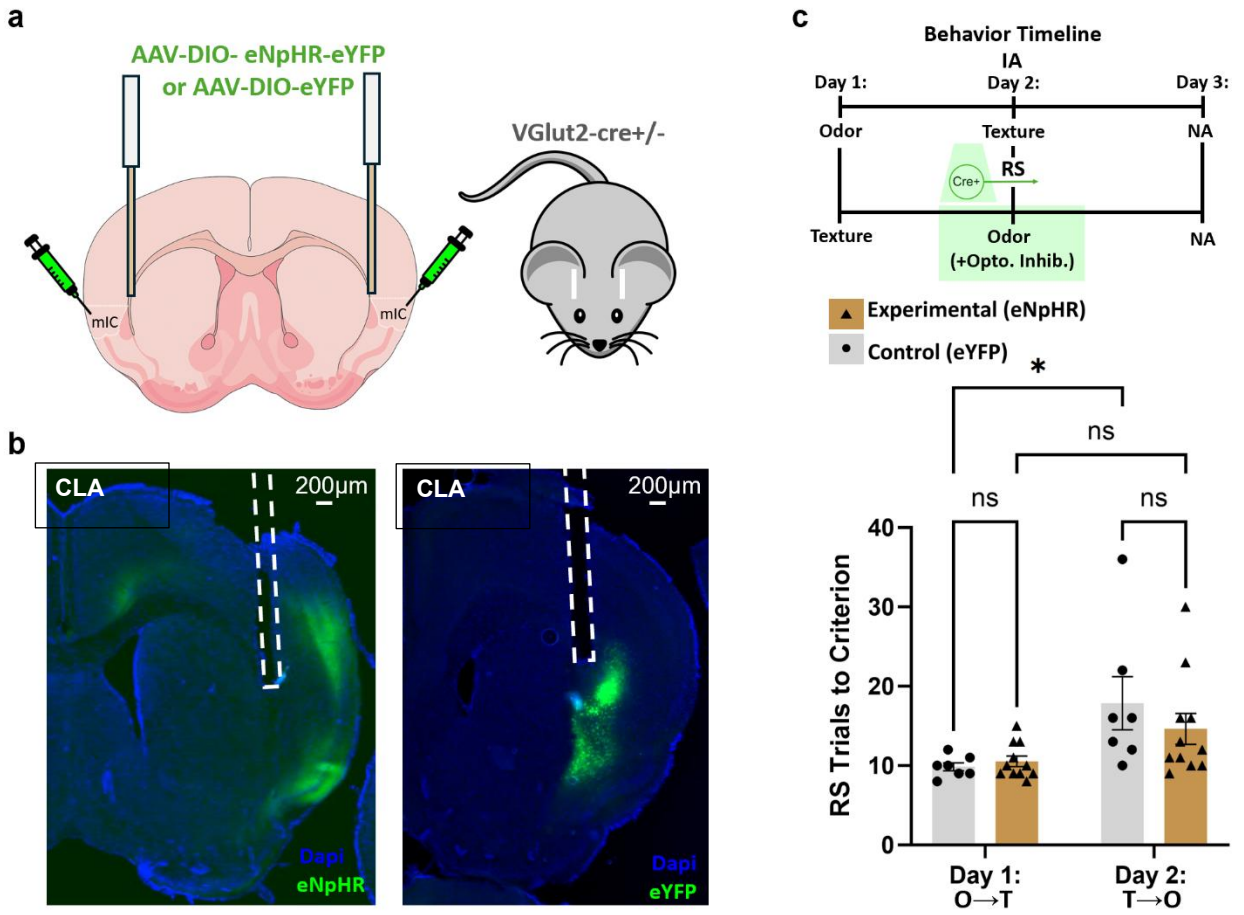

Figure 3.1: *Optogenetic Inhibition of the CLA during rule shift to odor*: a)Surgery schematic of injection of AAV-DIO-eNpHR-eYFP or AAV-DIO-eYFP injected bilaterally into CLA. b) Example of viral injection and implants (eNpHR on the left, eYFP right) from surgeries in (a). c) Top: the behavioral timeline where CLA cell bodies are inhibited during each trial on day 2 during rule shifts to odor; bottom: there is no significant deficit of during inhibition (Day 1 vs Day 2 Experimental (eNpHR): p=0.09; Day 1 vs Day 2 Control (eYFP): p=0.01; Day 2 Experimental (eNpHR) vs Control (eYFP): p=0.13).

Notably these changes in performance are similar in magnitude between experimental (eNpHR+) and control (eYFP+) mice, and much smaller than those observed when inhibiting the mIC. This suggests that optogenetic inhibition of the CLA does not produce marked impairments in behavior (beyond those caused by light delivery alone).

Chapter 4

Gamma Synchrony between mIC and mPFC

Now that we have determined that the mIC-mPFC projection is necessary for rule shifts to an odor-based rule, this raises the question of whether gamma oscillations in mIC and mPFC circuits synchronize during these rule shifts. Specifically, is there gamma synchrony between PVIs in the mIC and those in the mPFC, similar to the gamma synchrony our lab has observed between PVIs in the two mPFC hemispheres?[9] Furthermore, does any potential mIC-mPFC synchrony differ between shifts to odor vs. texture-based rules? If there is gamma synchrony, are there any long-range PVI projections from mIC to mPFC? Is any potential gamma synchrony between mIC and mPFC necessary for optimal rule shifting to odor?

Gamma synchrony between mIC and mPFC PVIs during TEMPO recording (shift to odor vs shift to texture)

To begin answering the above questions, we used Transmembrane Electrical Measurements Performed Optically (TEMPO) to measure gamma synchrony (30-50Hz) between mIC and mPFC PVIs. TEMPO uses genetically encoded voltage indicators (GEVIs) to measure voltage membrane dynamics at fast time scales comparable to LFP recordings but for specific cell types.[31] This allowed us to record oscillations from PVI in mIC and mPFC. To do so we injected PV-Flp mice in both the mPFC and mIC with AAV-fDIO-Ace-mNeon to express the GEVI, Ace-mNeon in PVIs, as well as AAV-syn-tdTomato to generate a control fluorophore signal. We implanted optical fibers for photometry unilaterally in both the mIC and mPFC (Fig. 4.1a-b).

For TEMPO recordings, mice were plugged into the fluorescence mini-cubes (FMC), which were connected to LEDs for providing excitation (490nm or 565nm), and photoreceivers for collecting the resulting emission from Ace-mNeon or tdTomato. Lock-in amplifiers were utilized to modulate LED excitation, demodulate corresponding photoreceiver outputs, and

remove noise with low pass filters (Fig. 4.1c; see methods). Mice were run on the Rule-Shifting task for two days, and we randomly counterbalanced whether they started with odor or texture-based rules on Day 1.

To precisely measure synchrony between mIC and mPFC we used an analysis technique described in Phensy et al, 2025. Briefly, a broad bandpass filter was applied to filter raw fluorescence signals between 1.6-78.4Hz. Subsequently, the resulting signals were filtered for gamma (30-50Hz) activity. Once the signals are filtered, there remains the possibility of noise such as movement or hemodynamic artifacts that could contaminate the signal from the GEVI, Ace-mNeon. As mentioned above, syn-tdTomato is used as a reference fluorophore. The syn-tdTomato signal remains constant but will fluctuate with unpredictable noise such as movement and hemodynamic artifacts. Therefore, to remove these artifacts from the Ace-mNeon signal, after the initial filtering, the best fit of the reference (tdTomato) signal to the voltage (Ace-mNeon) signal was subtracted from the filtered Ace-mNeon signal to yield a 'cleaned' Ace-mNeon signal (Fig. 4.1d). This is done for both mIC and mPFC recordings. We computed the cross correlation between mIC and mPFC signals to quantify gamma synchrony. We examined this metric of gamma synchrony during both pre- and post-decision periods (1-3s before the mouse starts to dig and the time between outcome and trial end) (Fig. 4.1e-j).

During the pre-decision period we observed different patterns of gamma synchrony between the mIC and mPFC during shifts to odor vs texture-based rules (Fig. 4.1e-g). During shifts to odor-based rules, correct trials have significantly greater gamma synchrony than error trials ($p=0.02$), but the reverse is true during shifts to texture-based rules (correct vs. error trial synchrony: $p=0.04$) (Fig. 4.1e). We also observed a significant difference between gamma synchrony on error trials during shifts to odor vs texture-based rules ($p=0.005$). This is consistent with the idea that there is a difference between mIC and mPFC coordination depending on the cue modality being used for decision making, and could be a possible mechanism explaining why inhibiting mIC-mPFC projections selectively impairs shifts to odor-

based cues.

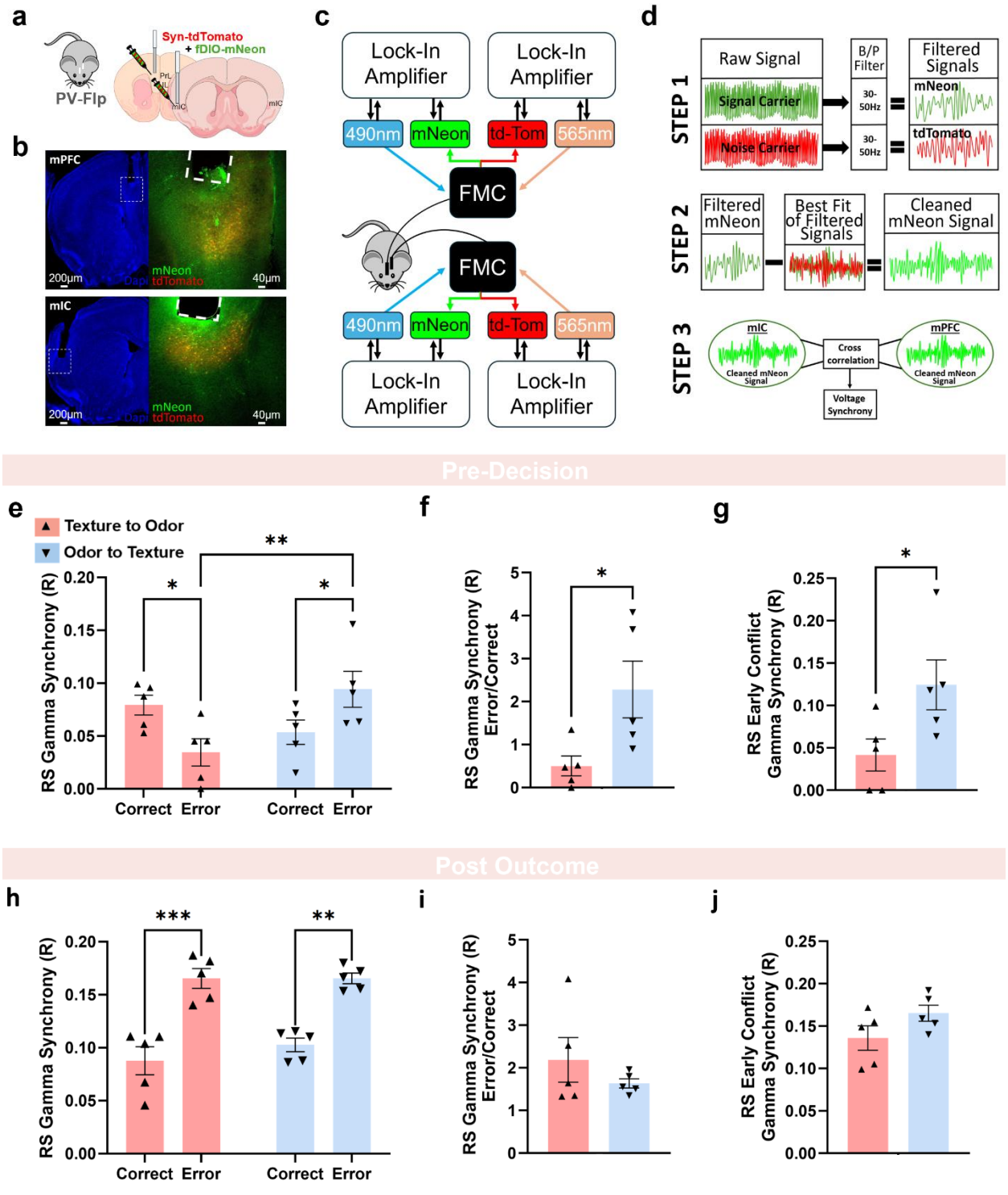

Figure 4.1: *Gamma synchrony between mIC and mPFC PV interneurons during **TEMPO** recording*: a)Surgery schematic of injection of a 2:1 dilution of AAV1-CAG-fDIO-Ace2N-4AA-mNeon and AAV2-Syn-tdTomato and optic fiber implant unilaterally. b) Example of viral injection and implants (mPFC on top, mIC on bottom) from surgeries in (a). c) Schematic of hardware set up, with dual-site fiber photometry mNeon and tdTomato signals were demodulated via lock-in amplifier. d) Gamma band activity is extracted by filtering raw fluorescent signals at 30-50Hz; cross correlation analysis is then performed on filtered signals to determine synchrony between mPFC and mIC. *(Figure continued on next page)*

(Figure continued from previous page) Looking at gamma synchrony during the pre-decision period e) there is a significant difference between correct and error trials for texture to odor (p=0.02) and odor to texture (p=0.04) shifts and a difference in error trials between odor and texture shifts (p=0.005). f) An overall difference between odor and texture shifts for normalized signal (error/correct; p=0.03) and g) a difference between odor and texture shifts during early conflict trials (p=0.03). Looking at gamma synchrony during the post outcome period h) there is a significant difference between correct and error trials for texture to odor (p=0.0004) and odor to texture (p=0.001) shifts and no significant difference in error trials between odor and texture shifts (p=0.20), i) no overall significant difference between odor and texture shifts for normalized signal (error/correct; p>0.99) and j) no significant difference between odor and texture shifts during early conflict trials (p=0.22).

The gamma synchrony for correct trials has no significant difference for the opposing RS error trials; this is interesting because it could serve as a predictive signal for the kind of rule the mouse expects a reward from. Above we saw the mIC is necessary for optimal shifts to an odor-based rule; it is possible that during correct trials for shifts to odor, the mouse needs to tap into information from the mIC and therefore increases the mIC-mPFC gamma synchrony to make the correct decision. Above we saw the mIC is NOT necessary for optimal shifts to texture RS; during correct trials for odor to texture, the mIC is not necessary which could be the reason for its lack in gamma synchrony compared to texture to odor correct trials (Fig. 4.1e). It is possible that during odor to texture shifts, instead a different brain region is being recruited to synchronize with mPFC; theoretically if that region was found, we may see identical results as Figure 4.1(e-g), with shifts to odor vs texture reversed.

When comparing an overall difference, or normalized signal, between shifts to odor and shifts to texture, error/correct, we continue to see a difference between texture to odor and odor to texture shifts (p=0.03). We again see a difference between these two shifts looking at early conflict trials (p=0.03).

During the post-outcome period (Fig. 4.1h-j) we see no difference between shifts to odor and shifts to texture for any trial types. We see a significant increase in gamma synchrony for error trials for both shifts to odor (p=0.0004) and shifts to texture(p=0.001) (Fig. 4.1h). This increase in gamma synchrony during error trials of the post decision period is also something we have seen among mPFC hemispheres which is necessary for learning[9]; leaving the possibility that this gamma synchrony between mIC and mPFC is necessary for learning shifts to odor. However, we do not see a significant difference in error trials between shifts to odor vs

texture(p=0.20) (Fig. 4.1h), difference in normalized signal (error/correct; p>0.99)(Fig. 4.1i) or difference between odor and texture shifts during early conflict trials (p=0.22).

Above we saw the mIC to mPFC projection is necessary only for an odor shift and not a texture shift, showing a difference between two cue type shifts; we continue to see a difference between these two cue types when looking at gamma synchrony between mIC and mPFC PVIs, further emphasizing this contrast.

Now that we understand the PVIs in the mIC and mPFC do have gamma synchrony, does that signify there are long-range PVI projections between mIC and mPFC? Is this gamma synchrony necessary for optimal rule shifts to odor?

Long-range mIC to mPFC projecting PVIs

We have established that there exists gamma synchrony between mIC and mPFC PVIs, and that mIC projections to mPFC are necessary for learning texture to odor rule shifts. This raises the question: do any PV+ mIC interneurons project to mPFC? If so, then these could directly coordinate gamma oscillations within the mIC and mPFC. If not, it would imply that the mIC PVIs likely exert their effects on mIC-mPFC gamma synchrony by influencing other mIC-mPFC neurons.

To explore this, we did a simple tracing study, by injecting a retrograde tracer (CTb-488), in the mPFC of PV-Cre/Ai14 mice (Fig.6a). One week later we perfused and sliced the brains to see if there is any overlap between CTb-labeled mIC-mPFC neurons and tdTomato-labeled PV+ neurons in mIC (Fig. 4.2b).

We found some PV+ neurons in mIC do overlap with mIC-mPFC neurons, suggesting that there are long-range-projecting mIC-mPFC PVIs (Fig. 4.2b). This could mean that PVIs in the mIC are not only influencing gamma oscillations in the mIC but also directly influencing gamma oscillations in mPFC. These long-range PVI projections could potentially be a driver of gamma synchrony between mIC and mPFC.

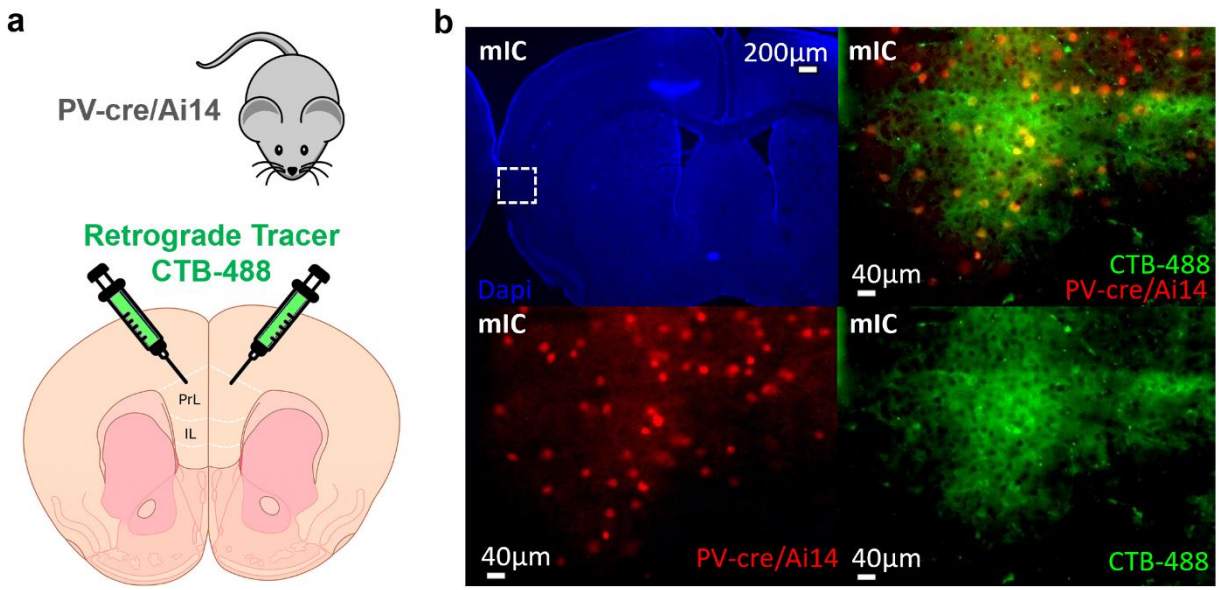

Figure 4.2: *Long-range mIC-mPFC PVIs*: a) Surgery schematic of injection of a retrograde tracer (CTB-488) injected into the mPFC. b) Example of overlap between tracer and CTB in mIC (Top left: slice including mIC/region of interest; Top right: in mIC, yellow signifies overlap of PVIs and mIC-mPFC neurons; bottom left: PVI in mIC; bottom right: mIC-mPFC neurons).

Regardless of how gamma synchrony between mIC and mPFC PVIs is generated, is the gamma synchrony these PVIs create necessary for rule shifts to odor-based rules?

mIC and mPFC PV-interneuron gamma synchrony is necessary for rule shifts to odor

We examined the effects of disrupting gamma synchrony between mIC and mPFC PV-interneurons by delivering optogenetic excitation to these two populations either in- or out-of-phase.

To target PVIs, we used PV-cre and WT mice for experimental and controls respectively. We injected AAV5-DIO-ChR2-eYFP bilaterally in the mPFC and mIC (Fig. 4.3a-b) and implanted a dual optic fiber in mPFC and optic fibers in mIC bilaterally. One concern is that the virus may spread to regions other than the mIC; however, given the placement of the implant is predominantly above mIC, we can assume the bulk of the PVIs being manipulated should be in the mIC.

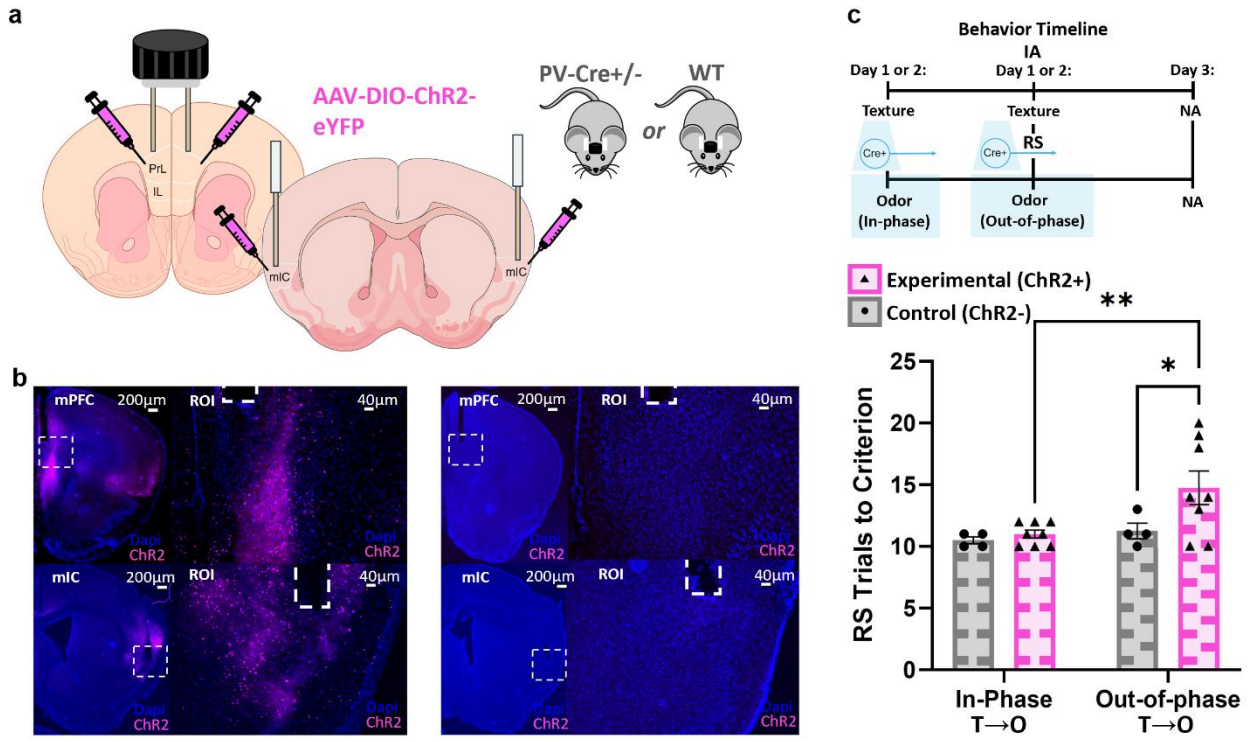

Figure 4.3: *mIC and mPFC PV-interneuron gamma synchrony is necessary for optimal rule shifts to odor*: a)Surgery schematic of injection of AAV-DIO-ChR2-eYFP and fiber implants bilaterally into mPFC and mIC. b) Example of viral injection and implants from surgeries in (a). c) Top: the behavioral timeline where mPFC and mIC PVI cell bodies are excited during each trial on day 2 during rule shifts to odor; bottom: there is a significant deficit between in-phase vs out-of-phase stimulation(Day 1 vs Day 2 Experimental (PV-cre): p=0.0057; Day 2 Experimental (ChR2) vs Control (WT): p=0.028; Day 1 vs Day 2 Control (WT): p=0.74).

After five weeks, we ran the rule-shifting task over two days (Fig. 4.3c). The IA cue was randomly assigned. Both days mice shifted from a texture cue to an odor cue while receiving bilateral optogenetic excitation in the mIC and mPFC. To mimic the zero phase lag gamma synchrony observed using TEMPO (Fig. 4.1), on one day, mice received in-phase 40Hz stimulation during RS trials. To disrupt this synchrony, on the other day, mice received out-of-phase 40Hz stimulation between the mIC and mPFC during RS trials. Note, optogenetic excitation was turned off when mice were in the holding cage during intertrial intervals (including extended timeouts after error trials). Mice were randomly assigned to receive either in- or out-of-phase stimulation on the first day, and received the other type on the following day.

We found that experimental (ChR2+) mice performed significantly worse during out-of-phase stimulation compared to in-phase (p=0.0057), as measured by an increase in the number

of trials to reach the learning criterion (8/10 trials correct) (Fig. 4.3c). Experimental (ChR2+) mice performed significantly worse than controls (ChR2-) during out-of-phase stimulation ($p=0.028$), whereas there was no significant difference between control and experimental mice when they received in-phase stimulation ($p=0.74$; Fig. 4.3c).

These results signify that the zero-phase lag gamma synchrony between mIC and mPFC PV-interneurons found in TEMPO during shifts to odor, is *necessary* for optimal rule shift learning.

Chapter 5

Discussion

Understanding the influence of individual cue types on cognitive flexibility, via the mPFC, may provide an understanding of their integration triggering adaptation for optimal environmental outcomes. Previous research has shown that the mPFC and its gamma synchrony are necessary for cognitive flexibility tasks such as the Rule-Shifting task.[7-9] While this research shows the necessity of gamma synchrony in the mPFC for cognitive flexibility, it does not parse out different cue types (ex: odor and texture) or explore the possibility of interregional gamma synchrony. Finding regions involved in enabling cognitive flexibility related to specific cue types and their involvement in gamma synchrony with the mPFC, will allow us to understand how the mPFC integrates different cues to form the necessary skill of environmental adaptation.

Here, we chose to observe the influence of the mIC on cognitive flexibility during the Rule-Shifting task and its relationship to the mPFC because of the mIC's involvement in cognition and known connectivity to the olfactory, somatosensory, and mPFC[20]. We found that mIC to mPFC projections are necessary for optimal Rule-Shifting, specifically to form texture to odor rule shifts. This necessity could be explained by the gamma synchrony between mIC and mPFC PVIs identified during TEMPO recordings. This projection's specificity for only texture to odor shifts may be explained by the difference in gamma synchrony found between the two types of shifts. Given that out-of-phase stimulation between the regions PVIs causes a detriment in texture to odor shifts, we conclude that the interregional gamma synchrony between the mPFC and mIC PVIs is necessary.

Through these experiments we have come closer to understanding one of the five sensory cues necessary for cognitive flexibility, aka odor, and it's need for interregional gamma synchrony. While this does not paint a full picture of how odor is integrated during cognitive

flexibility in the mPFC, it offers a significant start.

Some may argue we may not be testing the cue for odor at all, potentially testing odor and/or taste. However, the experience of taste is reliant on entering the mouth to stimulate taste receptors. During the Rule-Shifting task, we have not visually observed the mice eating or licking the media before deciding where to dig. It is possible when the mice dig up the reward there would be residual garlic or coriander powder on the pellet. However, during original preliminary data which optogenetically inhibited all mIC neurons during the RS trials, mice were handed a reward with tweezers, yet the impairment during a texture to odor shift was still present. Therefore, it is likely safe to infer that mice are in fact using an odor cue.

While this now shows the necessity of the mIC-mPFC projection and the synchrony between the mIC and mPFC, it does not explore the mPFC to mIC projection. Exploring this projection will allow us to understand the bidirectional circuit between mIC and mPFC and determine if one region is leading the gamma synchrony between them.

The above experiments also do not explore the impact the mIC has on the gamma synchrony between the mPFC hemispheres which is necessary for optimal cognitive flexibility.[7-9] In future experiments, with bilateral optogenetic inhibition in the mIC-mPFC projecting cell bodies with simultaneous TEMPO recordings bilaterally in mPFC, observing this will give us an understanding of how the mIC is impacting odor cognitive flexibility through the mPFC.

Based on my findings that the mIC-mPFC projection is necessary for texture to odor rule shifts (Fig. 2.1- 2.3), the necessity of PVI gamma synchrony between the two regions[30] (Fig. 4.1, 4.3), and the evidence of long-range PVI mIC-mPFC projections (Fig. 4.2), I propose the following *partial* schematic of the circuity between the mIC and mPFC which enables gamma synchrony (Fig. 5.1).

In figure 5.1, based on our current understanding, there is bidirectional connectivity between the mIC and mPFC[20]; PVIs project onto each other as well as onto pyramidal neurons[69] which are primary projection neurons,[70] making them a likely a part of the long-range

mIC-mPFC projection pathways, along with the long-range PVI projections (Fig. 4.2). Combining this information we have a partial idea of how the gamma synchrony between the mIC and mPFC occurs (Fig. 5.1). While figure 5.1 shows a partial schematic of the mIC and mPFC circuitry, to understand the circuit contributing to this gamma synchrony in its entirety, future experiments would need to explore the cell types mIC neurons project onto, mPFC to mIC projections and other cells types involved in long-range bidirectional projections.

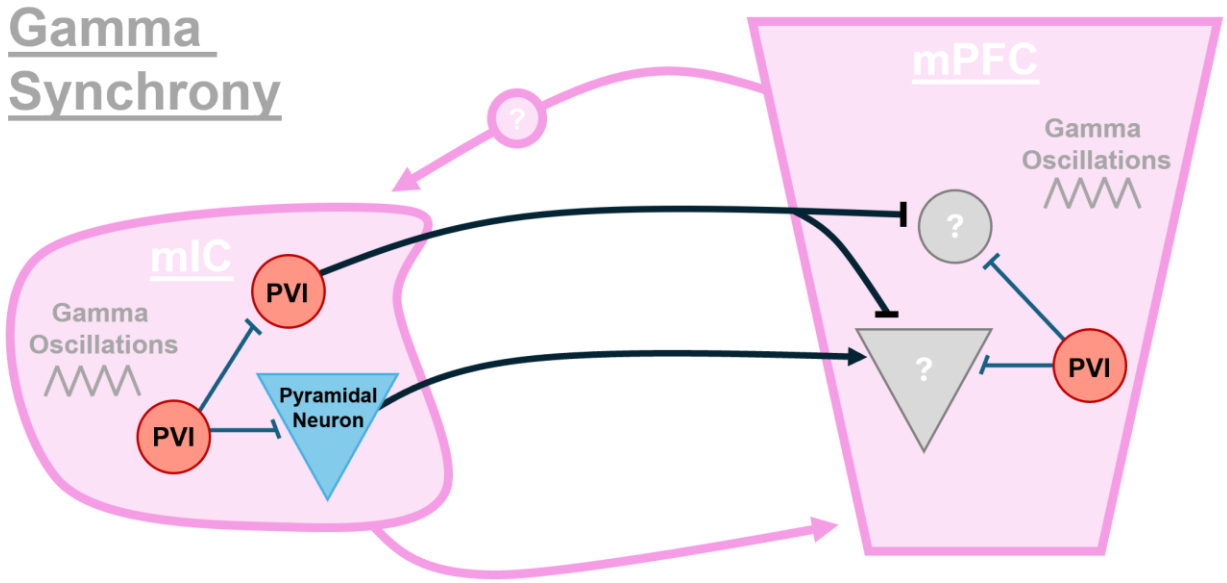

Figure 5.1: *Proposed partial schematic of mIC and mPFC circuitry causing gamma synchrony*: There exists bidirectional connectivity between mIC and mPFC.[20] Here, we are observing a proposed mIC-mPFC projection based on the necessity of mIC-mPFC neurons, *necessary* gamma synchrony between mIC and mPFC, and existence of PVI long-range projections.

For the first time we have identified a region that is necessary for shifting to a specific cue in the Rule-Shifting task, identified differences between the texture and odor cues in relation to gamma synchrony, and most shockingly shown the existence and necessity of gamma synchrony between the mPFC and mIC. This shows that gamma synchrony is not just important within a region, or regions adjacent to each other as previously observed,[9,29] but also necessary for interregional synchrony, showing a brand new role for gamma synchrony, previously only theorized.

Over all, this research has opened up many other questions. Does the mIC influence odor related learning or is it just rule shifting? Is the mIC the only region that would influence odor shifts? Would inhibiting the anterior IC have the same effect given it also contains the gustatory cortex as well as a larger percentage of cells that project to mPFC?[20] Is there a region specific for shifts to texture that also has necessary gamma synchrony with the mPFC? What other distant regions provide necessary gamma synchrony with the mPFC for optimal cognitive flexibility?

By gaining an understanding of how brain regions responsible for the cognitive flexibility of the five sensory cue types (sight, sound, taste, odor and tactile cues) influence gamma synchrony in the mPFC, we can create therapies that manipulate gamma oscillations. This could potentially help those with psychiatric or physiological conditions that impair their cognitive flexibility so they may properly take in cues, shift their behavior, and adapt to our continuously changing environment.

Chapter 6

Methods

Mice

NIH guidelines and a protocol approved by the Institutional Animal Care & Use Committee (IACUC) at the University of California, San Francisco were followed for all animal care, procedures and experiments. Mice were group housed (2-5 siblings) with full access to food and water in a normal 12hr light-dark cycle room kept at 22-24^{o}C until Rule-Shifting experiments began. All experiments used wild-type, PV-flp, and PV-flp/Ai14 lines on a C57Bl/6 obtained from Jackson Laboratories. Adult male and female mice were used, and were 8-12 weeks at the time of surgery and or 16-20 weeks old during behavioral experiments.

Cloning of Viral Constructs

Viruses pAAV-EF1a-Cre, AAV5-Ef1a-DIO-eNPHR-eYFP, and AAV5-Ef1a-DIO-eYFP were all purchased from Addgene. AAV2-Syn-tdTomato (1.23E+12 vg/mL) were purchased from SignaGen Laboratories.

We received AAV1-CAG-fDIO-Ace2N-4AA-mNeon (2.23E+13 vg/mL) from Mark J. Schnitzer (Stanford University) or the pAAV-CAG-fDIO-Ace2N-4AA-mNeon plasmid which was then packaged with stereotype AAV1 by Virovek (Houston, TX).

Surgery

All mice were anaesthetized using isoflurane (2.5% induction, 1.2-1.5% maintenance, in 95% oxygen) then placed on a stereotaxic frame (David Kopf Instruments) with a heating pad to maintain body temperature. The mouse's head was shaved with a electric razor and sterilized with ethanol and betadine. Lidocaine (1:4 dilution in saline) was injected underneath the scalp, and meloxicam (1:10 dilution) and Ethiqa XR were injected subcutaneously for analgesia. An incision was made to expose the skull. The scalp was pushed to the sides and periosteum was

removed from the dorsal skull surface. Necessary regions of the skull were drilled to create an opening for viral implants and/or injections. Using a micro-syringe pump (World Precision Instruments, UMP3 UltraMicroPump), viruses were infused at 100nL min through a 35-gauge, beveled injection needle (World Precision Instruments). The needle was kept at the injection site for 3-5min at the injection site post injection before being withdrawn. The skull was recleaned with saline. If needed, implants were placed one at a time in the desired areas, using Metabond Quick Adhesive Cement (Parkell).

mIC-to-mPFC cell body inhibition

For experiments using optogenetic inhibition of mIC-to-mPFC cell bodies, wild-type C57 mice were injected bilaterally in mPFC prelimbic and infralimbic cortices (1.7 AP; ±0.3 ML; -2.0, -2.25, -2.5 DV mm) and mIC (0.86 AP; ±3.4 ML; -4.0 DV mm) relative to bregma. In each hemisphere, the mPFC was injected with 3×0.2μL of the retrograde virus AAVrg-EF1a-Cre (Addgene). With a lateral facing needle, in each hemisphere, the mIC was injected with 600μL of AAV5-Ef1a-DIO-eNPHR-eYFP or AAV5-Ef1a-DIO-eYFP (Addgene). Implants with a 200/240μm (core/outer) diameter, NA=0.22 (Doric Lenses, MFC_200/240-0.22_2.8mm_ZF1.25(G)_FLT), were placed bilaterally in the mIC (0.86 AP; ±3.35 ML; -3.75 DV mm). To allow viral expression, all experiments began 8-10 weeks after surgery.

mIC to mPFC Terminal Inhibition

For mIC to mPFC terminal optogenetic inhibition experiments, wild-type C57 mice were injected bilaterally in the prelimbic and infralimbic regions of mPFC (1.7 AP; ±0.3 ML; -2.0, -2.25, -2.5 DV mm) and mIC (0.86 AP; ±3.4 ML; -4.0 DV mm) relative to bregma. In each hemisphere, mPFC received 3×0.2μL of the retrograde virus AAVrg-EF1a-Cre (Addgene). With a lateral facing needle, in each hemisphere, mIC received 600μL of AAV5-Ef1a-DIO-eNPHR-eYFP or AAV5-Ef1a-DIO-eYFP (Addgene). Implants with a 200/240μm (core/outer) diameter, NA=0.22 (Doric Lenses, MFC_200/240-0.22_2.8mm_ZF1.25(G)_FLT), were placed bilaterally in

the mPFC at a ±12º angle (1.7 AP, ±0.76, -2.14 DV). To allow viral expression, experiments began 8-10 weeks after surgery.

CLA to mPFC Cell body inhibition

For experiments using optogenetic inhibition of CLA-to-mPFC cell bodies, VGlut2+/- mice were injected bilaterally in CLA (0.86 or 1.1 AP; ± 2.85ML; -3.85 DV mm) relative to bregma. With a lateral facing needle, in each hemisphere, CLA received 600µL of AAV5-Ef1a-DIO-eNPHR-eYFP or AAV5-Ef1a-DIO-eYFP (Addgene). Implants with a 200/240µm (core/outer) diameter, NA=0.22 (Doric Lenses, MFC_200/240-0.22_2.8mm_ZF1.25(G)_FLT), were placed bilaterally in the CLA (0.86 or 1.1 AP; ±2.85 ML; -3.6DV mm). To allow viral expression, all following experiments began 8-10weeks after surgery.

TEMPO recording in mIC and mPFC

For mIC and mPFC PVI TEMPO experiments, PV-Flp mice were injected unilaterally in the left mPFC prelimbic and infralimbic cortices (1.7 AP; -0.3 ML; -2.0, -2.25, -2.5 DV mm) and left mIC (0.86 AP; -3.4 ML; -4.0 DV mm) (all coordinates relative to bregma) with a 2:1 mixture of virus to drive GEVI expression (AAV1-CAG-fDIO-Ace2N-4AA-mNeon; Schnitzer Lab) and AAV2-Syn-tdTomato (1.23E+ 12 vg/mL; SignaGen Laboratories) respectively. mPFC was injected with 3×0.2µL of this combination. With a lateral facing beveled needle, mIC was injected with 500µL of the same combination. Implants with a 400/430µm (core/outer) diameter, NA=0.48 (Doric Lenses, MFC_400/430-0.48_2.8mm_ZF1.25_FLT), were placed unilaterally in the left mPFC (1.7 AP; ±0.3 ML; -2.0 DV mm)and left mIC (0.86 AP; ±3.35 ML; -3.75 DV mm). To allow viral expression, experiments began about five weeks after surgery.

mIC and mPFC excitation

For mIC and mPFC PVI optogenetic in-phase and out-of-phase excitation experiments, PV-Cre+/- (experimental) and wild-type C57 (control) mice were injected bilaterally in mPFC prelimbic and infralimbic cortices (1.7 AP; ±0.3 ML; -2.0, -2.25, -2.5 DV mm) and mIC (0.86 AP; ±3.4 ML; -4.0 DV mm) (all coordinates relative to bregma). In each hemisphere, mPFC received

3×0.2μL of AAV5-EF1a-DIO-ChR2-eYFP. With a lateral facing beveled needle, mIC in each hemisphere was injected with 600μL of AAV5-EF1a-DIO-ChR2-eYFP. Dual fiber optic implants with a 200/240μm (core/outer) diameter, NA=0.22 (Doric Lenses, DFC_200/240-0.22_2.3mm_GS 0.7_FLT), were placed bilaterally in the mPFC. Fiber optic implants with a 200/240μm (core/outer) diameter, NA=0.22 (Doric Lenses, MFC_200/240-0.22_2.8mm_ZF1.25(G)_FLT), were placed bilaterally in the mIC (-0.21 AP; ±3.4 ML; -3.9 DV mm) at a 16° angle. To allow viral expression, experiments began 4-5 weeks after surgery.

Behavior

Rule Shifting Task

A detailed description of this task can be found in Cho et al., 2015. In this task, mice learn a rule or 'Initial Association' (IA) between a texture or odor cue and the location of a food reward, then switch to a new rule ('Rule Shift'; RS) based on a cue from the opposing modality. When performing this task, we were blind to genotype and/or virus injected.

Mice were placed with litter mates in a reverse light/dark cycle for 24-48 hours with normal food and water. Full diet 20mg food pellets (Dustless Precision Pellets, 20mg, Rodent Purified diet; Bio-Serv) were sprinkled into their cages during this time for them to acclimate to the new food. Then food deprivation begins.

Digging media was made by using odor causing ground dried spices (McCormick; garlic or coriander) were mixed with the media (~0.1% by volume), ground pellet powder was also mixed in (~0.01% of the volume).

Mice were singly housed in the same reverse light cycle for about a week. Food consumption was restricted to maintain mice at 80-85% of their pre-restriction weight by placing pellets in the middle of the media in two bowls, one filled with sand (Mosser Lee White Sand Soil Cover) with an odor of garlic or coriander, the other with litter (Natural Integrity Clumping Clay cat litter) with the other odor.

After 2-3 days of food deprivation, mice generally reach their target weight. They will

then be run through a ‘habituation’ protocol. During habituation mice run 10 consecutive trials with baited food bowls. In these trials, the mouse finds a reward while digging in all possible media combinations and each location (left or right) at least once. Mice are free to sample both bowls as they please until they find/eat the reward and are placed back into the holding cage. If mice fail to dig in the baited bowl, they are considered to have failed habituation, and this habituation protocol will be repeated the following day; if they fail again they are removed from the experiment.

On the following 2-3 days mice run the task. To determine which odor/texture combination and side (left or right) baited bowls will be placed on each trial, we used a custom MATLAB script that randomly assigns these values, with the requirement that the same odor/texture combination and side does not repeat on more than 2 trials consecutively.

In a given trial, a mouse is moved from the holding cage to its home cage where one of two bowls are baited; the mouse digs in a bowl and is then placed back into the holding cage. A trial is considered correct if the mouse digs in the baited bowl. The intertrial intervals for correct trials are about 10s while bowls are reset. A trial is considered incorrect when a mouse digs in the non-baited bowl; during this time, the baited bowl is removed and the mouse is free to dig in the non-baited bowl until it appears disinterested; the mouse is then moved to the holding cage for a 40s time out / intertrial interval.

On each day mice must first learn an initial association (IA) between one cue and the location of the hidden food reward. Once mice get 8/10 trials correct, they are considered to have learned the rule. If on a non-manipulation day, mice fail to learn the IA within 15 trials, they fail that day and are run again the next day; if they fail a second time they are removed from the experiment. Once IA is learned, the experimenter moves on to the rule-shift (RS); here the rule is shifted to the opposing modality (example: If the IA is based on an odor cue then the RS uses a texture cue and vise versa). Once mice get 8/10 trials correct, they are considered to have learned the rule-shift. Mice typically learn the IA in about 10 trials and the RS in about 10-15

trials.

For analysis described below, the onset of digging was considered the time of decision making. This was for two reasons. First, during an incorrect trial, once a mouse dug in the in the non-baited bowl, the baited bowl was removed. Second, digging was necessary to receive feedback of correct or incorrect choice based on the presence or absence of the reward.

For all behaviors, the experimenter was blind to which mice were experimental and which were control mice.

Optogenetic Inhibition

Continuous eNpHR stimulation was delivered during trials using a 532nm green laser coupled to two mono fiber-optic cannulas (Doric Lenses, Inc) through a 200μm diameter Splitter Branching Fiber optic patch cord with mating sleeves (Doric Lenses, Inc.). The final light power was adjusted to ~2.5mW for each branch (~5mW total across both branches). While the mouse was in the holding cage, before the start of a trial, the laser was manually turned on, and the mouse was placed in its home cage for the start of the trial. Once a mouse was placed back in the holding cage the laser was turned off; the laser remained off during any portion of the intertrial intervals, including time-outs.

Optogenetic Excitation (In-Phase vs. Out-of-Phase)

A 40Hz train of 5ms pulses was delivered to both fibers to produce in-phase stimulation. Out-of-phase stimulation was delivered using a 144 degree (10ms) offset between trains in the two fibers. ChR2 stimulation during trials was delivered via a 473nm blue laser coupled with two mono fiber-optic cannulas (Doric Lenses, Inc) through a 200μm diameter Splitter Branching Fiber optic patch cord with mating sleeves (Doric Lenses, Inc.). The final continuous light power, without 40Hz stimulation, was adjusted to ~1.3mW for each fiber (~5.2mW total across the four fibers). While the mouse was in the holding cage, before the start of each trial, the laser was manually turned on, and the mouse was placed in its home cage for the start of the trial. Once a mouse was placed back in the holding cage the laser was turned off; the laser remained off

during any portion of the intertrial intervals, including time-outs.

Histology and Imaging

All mice used for experiments were anesthetized with Euthasol. Then mice were transcardinally perfused with 0.01M PBS; once the blood ran clear mice were perfused with 4% paraformaldehyde (PFA) in PBS until muscle spasms stopped or the body was stiff. The brains were dissected and stored in 4% PFA over night at 4°C, then rinsed with PBS and transferred to 30% sucrose solution made in 0.01M PBS. At least 1-2 days were given for brains to sink before slicing. Brains were sliced at 60µm on a Leica SM2000 Microtome and mounted on slides with Fluoromount G with DAPI (Southern Biotech, Birmingham, AL). All imaging was performed on a BZ-X Series all-in-one fluorescence microscope (Keyance). We verified all mice had optical fibers, LFP electrodes and/or viral expression located in the proper regions.

Transmembrane Electrical Measurements Performed Optically (TEMPO)

Using the TEMPO technique described in Marshall et al., 2016, we measured time varying bulk fluorescence signals at each recording site (modifications below).

Optical Apparatus

Fiber optic implants with a 400/430µm (core/outer) diameter, NA=0.48 (Doric Lenses, MFC_400/430-0.48_2.8mm_ZF1.25_FLT), were sterotaxically implanted in the targeted region. A mouse was plugged in for recording using a fiber-optic patch cord (Doric Lenses, MFP_400/430/1100–0.48_2m_FC-ZF1.25) which was secured with a zirconia sleeve (Doric Lenses). This provided the light path between the mouse and a miniature, permanently-aligned optical bench, or ‘mini-cube’ (Doric Lenses, FMC5_E1(460–490)_F1(500–540)_E2(555–570)_F2(580–680)_S. Each fiber delivered excitation light and received emitted fluorescence from a recording site, and each recording site had its own implant, patch cord, mini-cubes, LEDs, photoreceivers and lock-in amplifiers.

Each mini-cube monitors two spectrally separate fluorophores. It does so by using dichroic mirrors and clean up filters that match the excitation and emission of the voltage sensor (‘Ace-mNeon’ voltage sensor channel: Excitation 460–490 nm, Emission 500–540 nm) and reference fluorophore (‘tdTomato’ control fluorophore: Excitation 555–570 nm, Emission 580–680 nm). Mini-cube optics were permanently aligned and sealed. Each cube has 5 ports; one sample port that plugs into the animal, two excitation and two emission lines. Each port has matching coupling optics and FC connectors.

The mini-cube was connected to fiber-coupled LEDs (Center wavelengths 490 nm and 565 nm, Thorlabs M490F3 and M565F3) via a patch cord (200 μm, NA=0.39; Thorlabs M75L01). LEDs were controlled using a 4-channel, 10kHz-bandwidth current source (Thorlabs DC4104), and the LED light intensity was adjusted to be ~200μW (Ace-mNeon) and ~100μW (td-Tomato).

Both emission ports on the mini-cube were attached to an adjustable-gain photoreceiver (Femto, Berlin, Germany, OE-200-Si-FC; Bandwidth set to 7kHz, AC-coupled, ‘Low’ gain of ~5×10^7 V/W) using a large-care high-NA fiber was used (600μm core, NA=0.48 (Doric lenses, MFP_600/630/LWMJ-0.48_0.5m_FC-FC)).

Modulation and lock-in detection

Each recording site had two LEDs. All four LEDs were sinusoidally modulated at distinct frequencies to reduce crosstalk between fluorophores with overlapping spectra. Lock-in amplifiers were used to demodulate corresponding photoreceiver outputs and remove noise using low pass filters. Each LED had a modulated waveform and demodulated the photoreceiver output at the carrier frequency through a single instrument (Stanford Research Systems, SR860). Each site had its own carrier frequency (mNeon site 1: 2 kHz; mNeon site 2: 2.5 kHz; Red site 1: 3.5 kHz; Red site 2: 4 kHz).

TEMPO recording

A multichannel real-time signal processor (Tucker-Davis Technologies, Alachua, Florida;

RX-8) was used for digitization. This signal processor was controlled using the software Synapse (Tucker-Davis Technologies) running on a windows PC. Synapse also saved the data into files on the PC and synchronized recordings with simultaneously acquired video from a USB webcam (Ailipu Technology, Shenzhen, China, ELP-USB100W05MT-DL36).

TEMPO Analysis

Methods for TEMPO analysis are described in previous work (Phensy, A.J. et al) but are briefly described here.

Videos were scored to identify timepoints corresponding to the trial start, dig start, outcome, and trial end. The pre-decision period is 1-3s seconds before the dig start based on the start of the trial; the post decision period is the time between the outcome and trial end.

Cross hemispheric gamma synchrony is quantified in PV-neurons using 250ms windows. First, following data acquisition, data was converted into a MATLAB structure using the SEV2Mat script from Tucker-Davis Technologies. Second, all signals were extracted: 1) left mIC mNeon, 2) left mIC tdTomato, 3) left mPFC mNeon 4) left mPFC tdTomato. Third, linear regression between broadband filtered (1.6-78.4Hz) mNeon and tdTomato signals was performed, to identify the shared noise component. This shared noise component was subtracted from the mNeon signal to ‘clean’ the signal; this allowed for non-voltage shared noise to be removed. Fourth, signals were band-pass filtered specifically within the gamma frequency band (30-50Hz) and an additional linear regression between mNeon and tdTomato was conducted to remove any additional noise. Lastly, the cross correlation of mIC and mPFC cleaned filtered signals were calculated across the entire session in 250ms windows to quantify gamma synchrony between the mIC and mPFC mNeon signals across the entire session. We identified when the peak of the cross-correlation was between -45 to 45 degrees and used these values to quantify ‘zero-phase lag’ mIC-mPFC PV interneuron gamma synchrony. All comparisons made were made by comparing these cross-correlation values.

Using these values, group comparisons were made using a mixed effects model or

paired nonparametric two tailed t-test. We corrected for multiple comparisons using statistical hypothesis testing (Tukey); if this correction was not possible due to 3 or less data points, each comparison stood on its own using a Fishers LSD test.

General Data Statistics for Behavior

Graphpad Prism 10 was used to conduct statistical analysis (see figure legends for details). Quantitative data are shown as the mean; error bars are used to represent the standard error of the mean (s.e.m.). Measurements were taken from distinct samples (*P* = *, < 0.05; **, <0.01; ***, < 0.001; ****, < 0.0001); no asterisk implied no significant difference (P>0.05). Sample sizes were based on number of mice available. Data distribution was assumed to be non-normal.

Group comparisons were made using a mixed effects model (all optogenetic inhibition and TEMPO), 2-way-ANOVA (optogenetic excitation), or paired non-parametric two-tailed t-text (TEMPO). If an interaction and/or a main effect was present, we corrected for multiple comparisons using statistical hypothesis testing (Tukey); if this correction was not possible due to limited data points, each comparison stood on its own using a Fishers LSD test.

References

1. Miller EK, Cohen JD. An integrative theory of prefrontal cortex function. Annu Rev Neurosci. 2001;24:167–202. doi: 10.1146/annurev.neuro.24.1.167.
2. Hosseini H, Evans-Martin S, Bogomilsky E, Jones KS. Grin2a dysfunction impairs cognitive flexibility by disrupting LC modulation of mPFC circuits. bioRxiv. 2025 Feb 1;2025.02.01.636062. doi: 10.1101/2025.02.01.636062.
3. Gläscher J, Adolphs R, Tranel D. Model-based lesion mapping of cognitive control using the Wisconsin Card Sorting Test. Nat Commun. 2019;10:20. doi: 10.1038/s41467-018-07912-5.
4. Klune CB, Jin B, DeNardo LA. Linking mPFC circuit maturation to the developmental regulation of emotional memory and cognitive flexibility. Elife. 2021 May 5;10:e64567. doi: 10.7554/eLife.64567.
5. Gruber AJ, Calhoon GG, Shusterman I, Schoenbaum G, Roesch MR, O'Donnell P. More is less: a disinhibited prefrontal cortex impairs cognitive flexibility. J Neurosci. 2010 Dec 15;30(50):17102-10. doi: 10.1523/JNEUROSCI.4623-10.2010.
6. Zhang Y, Shao F, Wang Q, Xie X, Wang W. Neuroplastic correlates in the mPFC underlying the impairment of stress-coping ability and cognitive flexibility in adult rats exposed to chronic mild stress during adolescence. Neural Plast. 2017 Jan 15;2017:9382797. doi: 10.1155/2017/9382797.
7. Cho KKA, Hoch R, Lee AT, Patel T, Rubenstein JL, Sohal VS. Gamma rhythms link prefrontal interneuron dysfunction with cognitive inflexibility in Dlx5/6+/− mice. Neuron. 2015;85:1332–1343. doi: 10.1016/j.neuron.2015.02.019.
8. Cho KKA, Davidson TJ, Bouvier G, Marshall JD, Schnitzer MJ, Sohal VS. Cross-hemispheric gamma synchrony between prefrontal parvalbumin interneurons supports behavioral adaptation during rule shift learning. Nat Neurosci. 2020;23:892–902. doi: 10.1038/s41593-020-0647-1.

9. Cho KKA, Shi J, Phensy AJ, Turner ML, Sohal VS. Long-range inhibition synchronizes and updates prefrontal task activity. Nature. 2023 May 11;617(7961):548-554. doi: 10.1038/s41586-023-06012-9.
10. Moghaddam AS, Mooziri M, Raoufy MR, Mirshekar MA. Olfactory bulb-medial prefrontal cortex circuit slow oscillations encode working memory representations. bioRxiv. 2025 Oct 30;2025.10.30.685257. doi: 10.1101/2025.10.30.685257.
11. Churchwell JC, Kesner RP. Hippocampal-prefrontal dynamics in spatial working memory: interactions and independent parallel processing. Behav Brain Res. 2011 Dec 1;225(2):389-95. doi: 10.1016/j.bbr.2011.07.045.
12. Peters AJ, Marica AM, Fabre JMJ, Harris KD, Carandini M. Visuomotor learning promotes visually evoked activity in the medial prefrontal cortex. Cell Rep. 2022 Oct 18;41(3):111487. doi: 10.1016/j.celrep.2022.111487.
13. Martin-Cortecero J, Nuñez A. Sensory responses in the medial prefrontal cortex of anesthetized rats. Implications for sensory processing. Neuroscience. 2016;339:109-123. doi: 10.1016/j.neuroscience.2016.09.045.
14. Euston DR, Gruber AJ, McNaughton BL. The role of medial prefrontal cortex in memory and decision making. Neuron. 2012 Dec 20;76(6):1057-70. doi: 10.1016/j.neuron.2012.12.002.
15. Tompary A, Davachi L. Integration of overlapping sequences emerges with consolidation through medial prefrontal cortex neural ensembles and hippocampal–cortical connectivity. eLife. 2024;13:e84359. doi: 10.7554/eLife.84359.
16. Skirzewski M, Molotchnikoff S, Hernandez LF, Maya-Vetencourt JF. Multisensory Integration: Is Medial Prefrontal Cortex Signaling Relevant for the Treatment of Higher-Order Visual Dysfunctions?. Front Mol Neurosci. 2022;14:806376. doi: 10.3389/fnmol.2021.806376.
17. DeNardo LA, Berns DS, DeLoach K, Luo L. Connectivity of mouse somatosensory and prefrontal cortex examined with trans-synaptic tracing. Nat Neurosci. 2015 Nov;18(11):1687-1697. doi: 10.1038/nn.4131.

18. Goswami R, Frances MF, Shoemaker JK. Representation of somatosensory inputs within the cortical autonomic network. NeuroImage. 2011;54(2):1211-1220. doi: 10.1016/j.neuroimage.2010.09.050.
19. Plakke B, Romanski LM. Auditory connections and functions of prefrontal cortex. Front Neurosci. 2014;8:199. doi: 10.3389/fnins.2014.00199.
20. Gehrlach DA, Weiand C, Gaitanos TN, Cho E, Klein AS, Hennrich AA, Conzelmann KK, Gogolla N. A whole-brain connectivity map of mouse insular cortex. Elife. 2020 Sep 17;9:e55585. doi: 10.7554/eLife.55585.
21. Silva-Filho JH, Pasian SR, do Vale FAC. Typical performance of elderly patients with Alzheimer disease on the Wisconsin Card Sorting Test (WCST). Dement Neuropsychol. 2007 Apr-Jun;1(2):181-189. doi: 10.1590/s1980-57642008dn10200011.
22. Han G, Helm J, Iucha C, Zahn-Waxler C, Hastings PD, Klimes-Dougan B. Are executive functioning deficits concurrently and predictively associated with depressive and anxiety symptoms in adolescents?. J Clin Child Adolesc Psychol. 2016;45(1):44–58. doi: 10.1080/15374416.2015.1041592.
23. Green MF. Cognitive impairment and functional outcome in schizophrenia and bipolar disorder. J Clin Psychiatry. 2006;67:36–42. doi: 10.4088/JCP.1006e12.
24. Rady A, Elsheshai A, Abou El Wafa H, Elkholy O. WCST Performance in Schizophrenia and Severe Depression with Psychotic Features. ISRN Psychiatry. 2012 Jan 23;2012:373748. doi: 10.5402/2012/373748.
25. Kang S, MacDonald AW, Chafee MV, Im C, Sponheim SR. Cortical Gamma Neural Synchrony Deficits in Schizophrenia Patients During Spatial Working Memory Task Performance. NeuroImage. 2009;47(S1):S136. doi: 10.1016/S1053-8119(09)71335-7.
26. Dzirasa K, McGarity DL, Bhattacharya A, Kumar S, Takahashi JS, Dunson D, McClung CA, Nicolelis MAL. Impaired limbic gamma oscillatory synchrony during anxiety-related behavior in a genetic mouse model of bipolar mania. J Neurosci. 2011 Apr 27;31(17):6449-6456. doi:

10.1523/JNEUROSCI.6144-10.2011.

27. Yin YY, Yan JZ, Lai SX, Wei QQ, Sun SR, Zhang LM, Li YF. Gamma oscillations in the mPFC: A potential predictive biomarker of depression and antidepressant effects. Prog Neuropsychopharmacol Biol Psychiatry. 2024 Feb 8;129:110893. doi: 10.1016/j.pnpbp.2023.110893.
28. Mimenza-Alvarado AJ, Aguilar-Navarro SG, Abarca-Jiménez IE, Vázquez-Villaseñor I, Luna-Umanzor DI, Dorard C, Villafuerte G. Low intensity gamma-frequency TMS safely modulates gamma oscillations in probable mild Alzheimer's dementia: a randomized 2 × 2 crossover pilot study. Front Neurol. 2025 May 15;16:1566476. doi: 10.3389/fneur.2025.1566476.
29. Sohal VS. How close are we to understanding what (if anything) γ oscillations do in cortical circuits?. J Neurosci. 2016 Oct 12;36(41):10489-10495. doi: 10.1523/JNEUROSCI.0990-16.2016.
30. Sohal VS, Zhang F, Yizhar O, Deisseroth K. Parvalbumin neurons and gamma rhythms enhance cortical circuit performance. Nature. 2009;459:698-702.
31. Marshall JD, Li JZ, Zhang Y, Gong Y, St-Pierre F, Lin MZ, Schnitzer MJ. Cell-type-specific optical recording of membrane voltage dynamics in freely moving mice. Cell. 2016 Dec 1;167(6):1650-1662.e15. doi: 10.1016/j.cell.2016.11.021.
32. Uddin LQ. Salience processing and insular cortical function and dysfunction. Nat Rev Neurosci. 2015 Jan;16(1):55-61. doi: 10.1038/nrn3857.
33. Menon V, Uddin LQ. Saliency, switching, attention and control: a network model of insula function. Brain Struct Funct. 2010 Jun;214(5-6):655-67. doi: 10.1007/s00429-010-0262-0.
34. Kusumoto-Yoshida I, Liu H, Chen BT, Fontanini A, Bonci A. Central role for the insular cortex in mediating conditioned responses to anticipatory cues. Proc Natl Acad Sci U S A. 2015 Jan 27;112(4):1190-5. doi: 10.1073/pnas.1416573112.
35. Ibañez A, Gleichgerrcht E, Manes F. Clinical effects of insular damage in humans. Brain Struct Funct. 2010 Jun;214(5-6):397-410. doi: 10.1007/s00429-010-0256-y.

36. Maffei A, Haley M, Fontanini A. Neural processing of gustatory information in insular circuits. Curr Opin Neurobiol. 2012 Aug;22(4):709-16. doi: 10.1016/j.conb.2012.04.001.

37. Bermudez-Rattoni F. The forgotten insular cortex: its role on recognition memory formation. Neurobiol Learn Mem. 2014 Mar;109:207-16. doi: 10.1016/j.nlm.2014.01.001.

38. Gogolla N, Takesian AE, Feng G, Fagiolini M, Hensch TK. Sensory integration in mouse insular cortex reflects GABA circuit maturation. Neuron. 2014 Aug 20;83(4):894-905. doi: 10.1016/j.neuron.2014.06.033.

39. Gogolla N. The insular cortex. Curr Biol. 2017;27(12):R580-R586. doi: 10.1016/j.cub.2017.05.010.

40. Hassanpour MS, Simmons WK, Feinstein JS, Luo Q, Lapidus RC, Bodurka J, Paulus MP, Khalsa SS. The insular cortex dynamically maps changes in cardiorespiratory interoception. Neuropsychopharmacology. 2018 Jan;43(2):426-434. doi: 10.1038/npp.2017.154.

41. Kayyal H, Chandran SK, Yiannakas A, Gould N, Khamaisy M, Rosenblum K. Insula to mPFC reciprocal connectivity differentially underlies novel taste neophobic response and learning in mice. eLife. 2021 Jul 5;10:e66686. doi: 10.7554/eLife.66686.

42. Uddin LQ, Nomi JS, Hébert-Seropian B, Ghaziri J, Boucher O. Structure and function of the human insula. J Clin Neurophysiol. 2017 Jul;34(4):300-306. doi: 10.1097/WNP.0000000000000377.

43. Méndez-Ruette M, Linsambarth S, Moraga-Amaro R, Quintana-Donoso D, Méndez L, Tamburini G, Cornejo F, Torres RF, Stehberg J. The role of the rodent insula in anxiety. Front Physiol. 2019 Mar 29;10:330. doi: 10.3389/fphys.2019.00330.

44. Chang LJ, Yarkoni T, Khaw MW, Sanfey AG. Decoding the role of the insula in human cognition: functional parcellation and large-scale reverse inference. Cereb Cortex. 2013 Mar;23(3):739-49. doi: 10.1093/cercor/bhs065.

45. Singer T, Critchley HD, Preuschoff K. A common role of insula in feelings, empathy and uncertainty. Trends Cogn Sci. 2009 Aug;13(8):334-40. doi: 10.1016/j.tics.2009.05.001.

46. Augustine JR. Circuitry and functional aspects of the insular lobe in primates including humans. Brain Res Rev. 1996;22:229–244.

47. Varjačić A, Mantini D, Levenstein J, Slavkova ED, Demeyere N, Gillebert CR. The role of left insula in executive set-switching: Lesion evidence from an acute stroke cohort. Cortex. 2018 Oct;107:92-101. doi: 10.1016/j.cortex.2017.11.009.

48. Ibañez A, Gleichgerrcht E, Manes F. Clinical effects of insular damage in humans. Brain Struct Funct. 2010 Jun;214(5-6):397-410. doi: 10.1007/s00429-010-0256-y.

49. Owen SF, Liu MH, Kreitzer AC. Thermal constraints on in vivo optogenetic manipulations. Nat Neurosci. 2019;22:1061–1065. doi: 10.1038/s41593-019-0422-3.

50. Smith JB, Lee AK, Jackson J. The claustrum. Curr Biol. 2020 Dec 7;30(23):R1401-R1406. doi: 10.1016/j.cub.2020.09.069.

51. Crick FC, Koch C. What is the function of the claustrum?. Philos Trans R Soc Lond B Biol Sci. 2005;360:1271–1279.

52. Zingg B, Dong HW, Tao HW, Zhang LI. Input-output organization of the mouse claustrum. J Comp Neurol. 2018 Oct 15;526(15):2428-2443. doi: 10.1002/cne.24502.

53. Kitanishi T, Matsuo N. Organization of the claustrum-to-entorhinal cortical connection in mice. J Neurosci. 2017 Jan 11;37(2):269-280. doi: 10.1523/JNEUROSCI.1360-16.2016.

54. Wang Q, Ng L, Harris JA, Feng D, Li Y, Royall JJ, Oh SW, Bernard A, Sunkin SM, Koch C, Zeng H. Organization of the connections between claustrum and cortex in the mouse. J Comp Neurol. 2017 Apr 1;525(6):1317-1346. doi: 10.1002/cne.24047.

55. Crick FC, Koch C. What is the function of the claustrum?. Philos Trans R Soc Lond B Biol Sci. 2005;360:1271–1279.

56. Marriott BA, Do AD, Zahacy R, Jackson J. Topographic gradients define the projection patterns of the claustrum core and shell in mice. J Comp Neurol. 2021 Apr 1;529(7):1607-1627. doi: 10.1002/cne.25043.

57. Baizer JS. The Neurochemical Organization of the Claustrum. In: Smythies JR, Edelstein LR, Ramachandran VS, editors. The Claustrum. Academic Press. 2014:85-118. doi: 10.1016/B978-0-12-404566-8.00003-9.

58. Jackson J, Karnani MM, Zemelman BV, Burdakov D, Lee AK. Inhibitory control of prefrontal cortex by the claustrum. Neuron. 2018 Sep 5;99(5):1029-1039. doi: 10.1016/j.neuron.2018.07.031.

59. Nahar L, Delacroix BM, Nam HW. The role of parvalbumin interneurons in neurotransmitter balance and neurological disease. Front Psychiatry. 2021;12:679960. doi: 10.3389/fpsyt.2021.679960.

60. Vidyasagar TR, Levichkina E. An integrated neuronal model of claustral function in timing the synchrony between cortical areas. Front Neural Circuits. 2019;13:3. doi: 10.3389/fncir.2019.00003.

61. Nunn J, Gregory L, Brammer M, Williams SC, Rogers J, Andrew C, Howard R, Baron-Cohen S, Bullmore E. Functional magnetic resonance imaging of synesthesia: activation of V4/V8 by spoken words. Nat Neurosci. 2002;5:371–375. doi: 10.1038/nn818.

62. Smythies J, Edelstein L, Ramachandran V. Hypotheses relating to the function of the claustrum. Front Integr Neurosci. 2012;6:53. doi: 10.3389/fnint.2012.00053.

63. Fodoulian L, et al. The claustrum-medial prefrontal cortex network controls attentional set-shifting. bioRxiv. 2020. doi: 10.1101/2020.10.14.339259.

64. Hur EE, Zaborszky L. Vglut2 afferents to the medial prefrontal and primary somatosensory cortices: a combined retrograde tracing in situ hybridization study. J Comp Neurol. 2005;483:351-373.

65. Goll Y, Atlan G, Citri A. Attention: the claustrum. Trends Neurosci. 2015 Aug;38(8):486-95. doi: 10.1016/j.tins.2015.05.006.

66. Phensy AJ, Hagopian LL, Costello CM, Haziza S, Ghenand O, Zhang Y, Schnitzer MJ, Sohal VS. Prefrontal gamma oscillations engage dynamic cell type-specific configurations to

support flexible behavior. bioRxiv. 2025 Sep 10;2024.03.08.584173. doi: 10.1101/2024.03.08.584173.

67. Jezzini A, Mazzucato L, La Camera G, Fontanini A. Processing of hedonic and chemosensory features of taste in medial prefrontal and insular networks. J Neurosci. 2013 Nov 27;33(48):18966-78. doi: 10.1523/JNEUROSCI.2974-13.2013.
68. Floresco SB, Block AE, Tse MT. Inactivation of the medial prefrontal cortex of the rat impairs strategy set-shifting, but not reversal learning, using a novel, automated procedure. Behav Brain Res. 2008 Jun 26;190(1):85-96. doi: 10.1016/j.bbr.2008.02.008.
69. Druga R, Salaj M, Al-Redouan A. Parvalbumin - Positive Neurons in the Neocortex: A Review. Physiol Res. 2023 Jul 31;72(Suppl 2):S173-S191. doi: 10.33549/physiolres.935005. PMID: 37565421; PMCID: PMC10660579.
70. Gerfen CR, Economo MN, Chandrashekar J. Long distance projections of cortical pyramidal neurons. J Neurosci Res. 2018 Sep;96(9):1467-1475. doi: 10.1002/jnr.23978. Epub 2016 Nov 12. PMID: 27862192; PMCID: PMC5429214.

Publishing Agreement

It is the policy of the University to encourage open access and broad distribution of all theses, dissertations, and manuscripts. The Graduate Division will facilitate the distribution of UCSF theses, dissertations, and manuscripts to the UCSF Library for open access and distribution. UCSF will make such theses, dissertations, and manuscripts accessible to the public and will take reasonable steps to preserve these works in perpetuity.

I hereby grant the non-exclusive, perpetual right to The Regents of the University of California to reproduce, publicly display, distribute, preserve, and publish copies of my thesis, dissertation, or manuscript in any form or media, now existing or later derived, including access online for teaching, research, and public service purposes.

DocuSigned by:
AA3030F3D1564F6...
Author Signature

05/21/2026
Date